Pergamon

Polyhedron Vol. 13, No. 8, pp. 1197–1223, 1994

0277–5387/94 $7.00+0.00

NANOSCALE MAGNETIC PARTICLES. NEW METHODS TO SURFACE PROTECTED METALLIC AND IMMISCIBLE BIMETALLIC CLUSTERS/PARTICLES

KATHIE A. EASOM, KENNETH J. KLABUNDE* and CHRISTOPHER M. SORENSEN

*Department of Chemistry, Kansas State University, Manhattan, KS 66506, U.S.A.

and

GEORGE C. HADJIPANAYIS

Department of Physics and Astronomy, University of Delaware Newark, DE 19716, U.S.A.

Abstract—The metal vapour–solvent low temperature matrix method has been used to prepare nanoscale iron powders. The morphology of the fine particles was characterized using transmission electron microscopy. Crystallite and particle sizes were determined via XRD and BET techniques. The magnetic properties of the powders were investigated using Mössbauer spectroscopy and SQUID magnetometry. X-ray photoelectron spectroscopy was used to probe the surface of the fine particles. The use of a non-polar solvent (hexane) to trap the atoms resulted in air-sensitive iron powders with some incorporation of carbon and hydrogen. Crystallite sizes of approximately 5 nm were observed and these systems behaved superparamagnetically at room temperature. The powders were easily oxidized to α-Fe_2O_3. Codeposition of iron with perfluorotri-n-butyl-amine (PFTA) resulted in the formation of FeF_2 as the major product. Reduced values of T_N and θ_c were observed for FeF_2 phase. The fine powders were found to be air and moisture sensitive forming FeF_3, $FeF_3 \cdot H_2O$ and γ-Fe_2O_3 upon exposure to air. The bimetallic system of immiscible metals, Fe and Ag, was investigated by co-deposition of these metals with pentane. Separate phases of Ag and Fe were observed to be in these powders. Mössbauer investigations indicated that isolated iron atoms accounted for 5–27% of the iron present indicating some solid solubility of these two metals. Enhanced hyperfine fields were observed for the iron clusters. Fe_3O_4, formed during handling of the powders, had reduced hyperfine fields for both A and B sites as well as reduced Verwey transition temperatures. Iron powders prepared in pentane and trapped with 1-dodecanethiol exhibited unique behaviour after heat treatment. Small iron particles with a coating of FeS were formed after heat treatment at 300–600°C for 2 h under argon. Air sensitivity of the powders was greatly reduced after the formation of the sulphide surface layer. The possible existence of exchange interactions between the two phases was investigated using magnetic measurements and was found to be small but significant. These experiments demonstrate that metal atom clustering in low temperature matrices, followed by trapping/ligation and or heat treatment can yield a variety of new nanoscale materials. Crystallite sizes and outer coating material can be controlled and manipulated. Immiscible bimetallic particles, core-shell structures, and many other unique phases are attainable.

INTRODUCTION

Interest in ultrafine particle research has grown in recent decades as researchers attempt to characterize the novel properties of these materials. Clusters with sizes 1–100 nm have been shown to have unique, hybrid properties which are different from that of either the molecular or the bulk solid size limits. Research into the growth and properties of small clusters spans many areas of interest such as

*Author to whom correspondence should be addressed.

biological systems,[1] catalysis,[2] electronic materials,[3] and magnetic materials.[4]

Various techniques for the preparation of fine powders have been described in the literature such as vacuum synthesis, gas phase synthesis and condensed phase synthesis. We chose to prepare fine iron particles by the solvated metal atom dispersion (SMAD) technique. This method allows for the solvent moderated growth of ultrafine particles in organic media. Particles prepared by this method have been shown to possess unique catalytic[5] and magnetic properties.[6]

The iron system was chosen, in part, due to the high value of saturation magnetization (220 EMU g^{-1}) of the bulk material.[7] We hoped to prepare fine particles of iron having higher coercivities than those observed for fine particle iron oxides, for which the saturation value is lower.[8] These studies have applications in the field of information storage where the demand for high quality, high density recording media is increasing. .

The challenge in preparing and characterizing iron fine particles is their susceptibility to oxidation. Indeed, a drawback to the use of these particles in recording materials is the corrosion processes which occur over time. One protective measure is coating the particles with a surface layer of oxide, but this also serves to reduce the magnitude of the saturation magnetization by 30–40%.[9] We investigated three methods of preparing protected iron particles: (1) preparation of the particles in a fluorinated solvent, (2) preparation of bimetallic Fe/Ag powders and (3) preparation of the particles in pentane followed by trapping with an organic thiol.

BACKGROUND INFORMATION

Fine particle research

As scientists attempt to understand the properties of nanoscale materials, methods of preparing macroscopic amounts (gram quantities) of these powders have been developed. These methods can be divided into two broad categories: gas phase synthesis, and condensed phase synthesis.

The technique of gas phase synthesis typically involves aggregation of atoms or clusters in the presence of an inert gas.[10] The inert gas serves to remove the heat of condensation of the clusters as they grow and can also serve to control ultimate particle size by proper choice of gas and gas pressure. The monomer population may be established by use of a heated crucible,[10a] by laser vapourization[11] or by laser pyrolysis[12] or sputtering.[13]

Laser vapourization has been used to produce clusters of semiconductors,[14] transition metals,[15] and main group metals.[16]

This technique can be extended to alloy targets[17] or to the preparation of mixed clusters which normally do not alloy.[18] While laser vapourization is a versatile method of producing clusters it still has the limitation of producing a small amount of material per unit time.

Laser pyrolysis is a useful technique for synthesizing fine powders of refractory materials. For example, ultrafine powders of SiC[12a] and TiO_2[12b] were produced by heating a flowing mixture of reactant gas and an inert carrier gas. The gas phase decomposition of reactant produced a vapour of the desired atoms which grew to clusters while being cooled by collisions with the carrier gas. The formation of more complex refractory materials can be accomplished by using a volatile organometallic compound. For instance, 100 nm spheres of Si/N/C have been synthesized by the pyrolysis of $(Me_3Si)_2NH$.[19]

Condensed phase synthesis (of nanoscale materials)

Includes precipitation reactions,[20] growth within micelles,[21] growth within zeolites,[22] and growth in low temperature organic solvents.[23]

Precipitation reactions have been used to prepare ultra-fine powders of metals[20a] and metal oxides[20b–d] in gram quantities. Matijevic and coworkers[20b] were able to prepare uniform hematite particles by aging a solution of ferric chloride at 100°C for 24 h. Hamada and coworkers[20c] modified this procedure by adding a chelating agent to the ferric chloride solution. They obtained dumbbell shaped hematite particles. The addition of a small amount of phosphate led to the formation of spindle type particles.[20d]

Fine particles of diameter less than 5 nm have been prepared in micelles and reversed micelles (microemulsions). Salts of platinum, palladium, and iridium have been reduced after being dissolved in microemulsions.[21a,b] Nickel and iron borohydride particles possessing high catalytic activity have also been grown in micelles.[21c] These systems generally produce monodisperse particles with the upper limit on particle size being determined by micelle cavity size.

Zeolites provide a three-dimensional framework in which nanoscale particles can be formed. For example, Zeolite Y, an aluminosilicate, has two sites available for cluster formation.[22a] One site is a 0.6 nm cage formed by sodalite units and the second site, the alpha cage, is 1.3 nm in diameter.

In particular, Zeolite Y has been used to prepare GaP_x particles by the reaction of $(CH_3)_3Ga$ and PH_3

within the pores.[22b] Extended X-ray absorption fine structure spectroscopy (EXAFS) and X-ray diffraction data suggest that the GaP_x particles were approximately 1.1 nm in diameter and the orientation of the cluster varies from cage to cage.

A final example of condensed phase synthesis is the SMAD technique. Using this method, it has been possible to prepare colloidal suspensions of metal clusters in organic solvents,[23a,b] highly reactive metal powders,[23c] and bimetallic clusters.[23d,e,f] This technique involves deposition of metal atom vapours into a freezing organic solvent. Upon warming, atoms and/or clusters migrate within the solvent and coalesce forming larger particles. By including a surfactant in the organic phase, it was possible to prepare air stable, nanoscale magnetic materials and colloidal magnetic fluids.[23g]

Preparation of iron fine powders

A variety of methods have been used to prepare nanoscale iron particles and a brief review of these techniques follows.

Bean and Jacobs[24] prepared small iron particles in Hg by electrolytic deposition. The mercury served as the cathode in their system. The particles had an average diameter of 4.5 nm and were protected from oxidation by the liquid mercury in which they were suspended.

Colloidal iron was synthesized by Nakatani and coworkers[25] by vacuum evaporation of bulk iron in a rotating cryostat. A thin film of oil (alkylnaphthalene) containing butenylsuccinpolyamine as a surfactant was used to trap and protect the fine particles. Uniform sized iron particles having diameters of 2.0 nm were isolated from the colloids. The magnetic fluid also contained a small amount of Fe_3O_4 after the colloid was heated. These magnetic fluids were reported to be stable towards aggregation for more than 1 year.

A widely used technique for preparing iron fine powders is by evaporating iron metal into an inert gas atmosphere,[26–29] at pressures ranging form 0.5 to 30 torr. Particle size could be controlled by regulating the gas pressure and iron particles were produced with sizes ranging from 10–100 nm in diameter. Oxidation of the powders was inhibited by embedding the particles in paraffin[26] or by the formation of thin oxide layer on the surface of the particles.[27–29]

The decomposition of $Fe(CO)_5$ has been used to prepare iron particles having a calculated mean particle diameter of 2.0–4.5 nm.[30] The decomposition was carried out by physisorbing $Fe(CO)_5$ on graphite at ambient temperature and then heating the sample to 378 K under dynamic vacuum. All subsequent handling of the particles occurred under vacuum, therefore no other precautions were employed to prevent oxidation.

Suslick and coworkers[31] reported that sonolysis of $Fe(CO)_5$ yielded nearly pure, amorphous iron powder having particle sizes of less than 10 nm. High catalytic activity of this powder was attributed to the high surface area which was roughly 150 times larger than that of the commercially available iron powder.

Ferromagnetic behaviour

The origin of magnetism in transition metal ferromagnets can be described using the band theory of solids.[32] When applied to magnetic materials, this theory is sometimes called the collective-electron theory or the itinerant electron theory. The following criteria for the existence of ferromagnetism have been established.

(1) There must be electrons in partially filled energy bands so that vacant energy levels are available for electrons with unpaired spins to move into.
(2) The density of levels in the band must be high so that spin alignment results in only a small increase in energy.
(3) The crystal lattice must have the proper spacing so that *d*-electron spins in one atom can align the spins in a neighbouring atom.

Iron, cobalt, and nickel satisfy all of the above conditions.

The electrostatic forces which cause spin alignment in these metals are called exchange forces.

With increasing temperature, thermal agitation works against the exchange forces and ferromagnetism disappears at a certain critical temperature. Above this temperature (T_c, Curie temperature) ferromagnets become paramagnets. Antiferromagnetic materials have a critical temperature, the Neel temperature (T_N), above which the antiferromagnetic ordering is disrupted and paramagnetism sets in.

Due to the existence of these exchange forces, it may be expected that all ferromagnetic materials would be spontaneously magnetized to saturation at temperatures below the Curie point. This is not usually the case, and it was Weiss who first predicted the existence of domains within the bulk material as an explanation for this.[33]

Domains are small regions within the specimen which are each spontaneously magnetized to saturation but which are oriented in such a way that the sample as a whole has a reduced magnetization. The formation of domains within a ferromagnetic material can be related to the existence of demag-

netization (stray) fields within the bulk. By dividing the specimen into smaller domains, the stray field is confined to smaller and smaller regions near the surface. This has the effect of confining the demagnetizing field to regions near the end of the specimen, and serves to reduce the effect over most of the volume of the specimen. So, even though the saturated state would minimize exchange energy, the sum of exchange and demagnetizing energies would not be a minimum for a uniformly magnetized specimen. The existence of domain walls has been established by TEM, XRD, and the Bitter techniques.[34]

There is a third energy consideration for ferromagnets which is termed the anisotropy energy, E_a. There are several kinds of anisotropy which contribute to this energy term: crystal, shape, stress exchange and induced anisotropy. Of these, only crystal anisotropy is intrinsic to the material. The anisotropies which will be pertinent to later discussions are reviewed below.

For single crystals of α-Fe, it has been shown that it is easier to saturate the sample when a magnetic field is applied parallel to the ⟨100⟩ direction.[37] Much higher fields are required to rotate the magnetization vector such that it is parallel to the ⟨111⟩ direction. The ⟨100⟩ and ⟨111⟩ directions are respectively termed "easy" and "hard" directions of magnetization for the iron crystal. Crystal anisotropy can be regarded as the force which tends to bind the magnetization to a certain direction of the crystal. The physical origin of this anisotropy is spin-orbit coupling of the electron and strong coupling of the electron orbit to the crystal lattice.

Shape anisotropy exists in non-spherical samples. Consider the case of an prolate spheroid with a major axis c and a minor axis a. If the sample is magnetized at some angle θ relative to c, then the demagnetizing fields which exist create a magnetostatic energy term. The equation which describes the magnetostatic energy is:

$$E_{ms} = 1/2M^2N_c + K_sM^2\sin\theta,$$

where N_a and N_c are the demagnetizing coefficients along a and c, respectively. K_s is the shape anisotropy constant and is equal to $1/2(N_a - N_c)M^2$. E_{ms} has a direction dependent term as was seen in the description of crystal anisotropy. In effect, the long axis of the prolate spheroid behaves as the easy axis of the crystal.[32] The strength of the shape anisotropy depends on the axial ratio c/a as well as on the degree of magnetization.

A third type of anisotropy arises in some small particle systems. It was first observed by Meiklejohn and Bean[36] who called it exchange anisotropy. These researchers noticed that fine particles of Co which are coated with a layer of CoO exhibited a shifted hysteresis loop when cooled in an applied field through the Neel temperature (T_N) of CoO. Samples which were not field cooled exhibited a normal, symmetrical hysteresis loop.

The unusual properties of the field cooled Co/CoO particles was due to exchange coupling between the spins of ferromagnetic Co and antiferromagnetic CoO at the interface of the two layers. Field cooling of the powders caused alignment of the first layer of Co ions in the oxide adjoining spins in the metallic core. As the sample was cooled below T_N antiferromagnetic ordering occurred in the oxide layer. If a reverse field was then applied, the spins in the cobalt reversed and the exchange coupling at the interface served to reverse the spin system of the oxide layer. This rotation was resisted by the strong crystal anisotropy of the cobalt oxide. Only partial rotation of spins occurred. The result was a larger negative coercive field was required to demagnetize the sample giving a shifted hysteresis loop. Because the anisotropy is unidirectional, not uniaxial, the energy depends on the first power of the cosine:

$$E = -K\cos\theta,$$

where K is the exchange anisotropy constant and θ is the angle between M_s and the direction of the cooling field.

The three requirements for exchange anisotropy are:

(1) Field cooling through T_N.
(2) Intimate contact between ferromagnetic and anti-ferromagnetic phases.
(3) Strong crystalline anisotropy in the antiferromagnet.

Exchange anisotropy has also been observed in single phase systems such as disordered Ni_3Mn solid solutions.[37]

The hysteresis loop

Application of a magnetic field, H, to a demagnetized sample will cause an increase in magnetization as illustrated in Fig. 1.[38] Starting from point O, the magnetization increases to point A. Further increases in the applied field past point A causes no more change in sample magnetization. The sample is now saturated and the saturation magnetization is equal to the spontaneous magnetization described earlier.

If the applied field is decreased, the sample magnetization does not follow the curve A–O but instead M decreases slowly to point B. At zero applied field the sample retains a non-zero magnetization. Application of a reverse field causes M

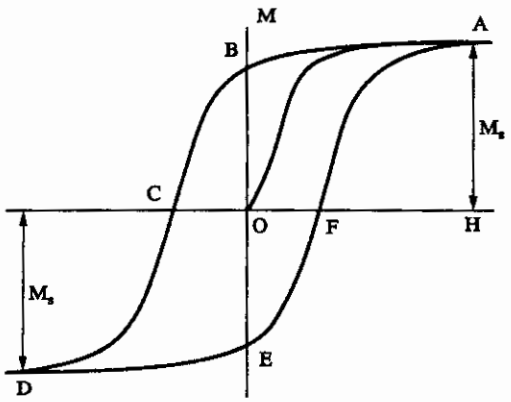

Fig. 1. Hysteresis loop of a ferromagnetic material.[38] Points A–F are described in the text. Magnetization (M) at saturation (M); O is at zero field; and H is applied magnetic field (positive to the right and negative to the left).

to pass through zero (point C) and finally to saturate again (point D). If H is decreased again, the magnetization will follow the curve D→E→F→A. Repeated variation in H between large values in opposite directions will cause M to vary repeatedly along this closed loop. This loop is termed the major hysteresis loop and the curve O→A is called the initial magnetization curve.

The important parameters used to describe the hysteresis loop are remanent magnetization (remanence), M_r and the coercive field (coercivity), H_c. The remanence is the largest magnetization the sample will give in zero field corresponding to points B and E in Fig. 1. The coercive field is the reverse field required to bring the sample magnetization to zero from remanence (points C and F).

Fine particle magnetism

In 1930, Frenkel and Dorfman predicted that a particle of ferromagnetic material below some critical size would behave as a single magnetic domain.[39] The critical size for single domain behaviour is now known to depend upon several factors: the strength of the crystal anisotropy present in the material, the value of the saturation magnetization, and the particle shape. Strong crystal anisotropy, in general, leads to larger single domain sizes whereas high M_s values lead to smaller sizes because of larger magnetostatic energies. This magnetostatic energy can be reduced if the particles are elongated along one axis.[32] For instance, calculations have shown that rod shaped particles of α-Fe with a length to diameter ratio of 10:1 have a critical diameter of about 100 nm (0.1μ).[40]

A collection of single domain particles which have negligible magnetic interactions can reverse their magnetization only by rigid rotation of the magnetization vector of each individual particle. As compared to the bulk material, which reverses magnetization by domain wall displacement at low fields, rigid (coherent) rotation requires large reverse fields so as to overcome any anisotropies (shape, crystal, stress) which oppose the rotation.[41]

By limiting the mode of magnetization reversal to coherent rotation only, it has been possible to manufacture fine particles of ferromagnetic materials having large coercivities.[20a,32] This is especially important when manufacturing materials for information storage where spontaneous erasure must be avoided. However, there is a limit to the observed increase in H_c with decreasing particle size. Carmen[42] reported a maximum in the coercivity of iron for particles 25.0 nm in diameter while Luborsky and Paine[43] found the maximum occurring at a size of 13.0 nm and having a value of 1050 Oe. Below these limiting sizes H_c decreases and superparamagnetism sets in.

Superparamagnetic behaviour was first described by Neel.[43] This behaviour is observed for single domain particles which are so small that thermal energy is sufficient to equilibrate the magnetization of an assembly over a time scale shorter than the time of the experiment. The particles behave similarly to paramagnets, but rather than having a small moment of a few Bohr magnetons, the moment is a sum of the moments of all of the atoms in the particle.

For a system of single domain ferromagnetic particles, in the absence of an applied field, there will exist two easy directions separated by an energy barrier KV, where K is the total anisotropy constant and V is the particle volume. When $KV < kT$ then thermal energy will induce fluctuations of magnetization within the particles and the fluctuation will have a characteristic time, τ_N, given by:

$$\tau_N = f_o \exp(-KV/kT),$$

The frequency factor, f_o, is related to the Larmor precession frequency and is approximately 10^{-8}sec^{-1}. The system is considered superparamagnetic when $KV \approx 25kT$ corresponding to a time of measurement of 100s. Below a critical temperature T_B, the blocking temperature, superparamagnetic behaviour disappears.

The magnetization of superparamagnetic particles obeys a Langevin law and can be expressed as:

$$M/M_s = \coth(\mu H/kT) - kT/\mu H,$$

which is also valid for paramagnetic systems where μ is the atomic moment rather than the moment of a particle. As a result, superparamagnetic materials will exhibit no hysteresis and will have temperature dependent properties such that magnetization curves obtained at different temperatures will superimpose when plotted against H/T.

Because of the exponential dependence of τ_N on particle volume, there is a well defined particle size at which transition to stable, single domain behaviour occurs. For a spherical iron particle having only crystalline anisotropy, a particle having a diameter of 11.5 nm will have a relaxation time of 10^{-1}s at room temperature and will behave as a super-paramagnet.[45] Increasing the size to 15.0 nm yields a relaxation time of 10^{9}s at room temperature so a collection of particles of this size would be extremely stable.

Bean and Livingston have calculated the critical radius for spherical Fe particles having blocking temperatures equal to room temperature.[45] They estimate a diameter of 12.5 nm if only crystal anisotropy is considered. For superparamagnetism to exist at 77 K a particle size of less than 8.0 nm is required. When the calculation was carried out assuming an elongated particle of Fe, the critical volume was estimated to be equivalent to that of a 3.0 nm sphere. Experimentally, they observed superparamagnetism for 77 K for Fe particles, having an average diameter of 4.4 nm, suspended in Hg. Measurements at 4.2 K indicated that some of the particles were stable as evidenced by the onset of hysteresis.

The temperature dependence of the magnetic behaviour of superparamagnetic materials can be used to estimate particle size and to deduce blocking temperatures.[24] However, these calculations assume that there are no interactions between the individual particles. When neighbouring particles are in contact, exchange anisotropy will exist at the interface between the particles.[46] If the particles are in close proximity to each other, dipole interactions will occur between their magnetic moments. Thus, the moments of these atoms will tend to align. These factors will serve to change the total anisotropy of the particles causing an apparent increase in the blocking temperature.

Clustering of particles can also change the initial slope of the magnetization curve.[24] Since these data are used to estimate individual particle size, care must be taken when interpreting such data if clustering or a particle distribution is believed to exist within the sample. For these cases, the law of approach to saturation is a better method for particle size estimation.

Mössbauer spectroscopy and fine particles

The Mössbauer effect may be described as the recoil-free emission and resonant absorption of γ-rays by the nuclei of atoms. The nuclear processes producing this effect were first reported by Rudolf L. Mössbauer in 1958.[47] Many review articles have been written which address the theory of Mössbauer spectroscopy and the type of information which can be obtained from these spectra.[48-51] The following discussion was drawn from these sources.

Normally, a Mössbauer spectrum is produced by varying the source γ-ray energy and measuring the nuclear resonance absorption as a function of γ-ray energy. Absorption will occur only when the γ-ray energy matches the nuclear excitation energy in the absorber. The energy of the source γ-ray is modulated by moving the source relative to the absorber thereby causing a Doppler shift in the energy.

The Mössbauer effect is only observed in solids or frozen liquids for which recoil-free resonant absorption of γ-rays is possible. The probability that a recoil-free transition will occur (in source or absorber) depends, in part, on the recoil-free fraction f. The expression for f is as follows:

$$f = \exp(-4\pi^2\langle x^2\rangle/\lambda^2)$$

where $\langle x^2\rangle$ is the mean square displacement of the nucleus in the direction of the emitted γ-ray and λ the wavelength of the γ-ray (0.86 Å for the 14 keV γ-ray of ^{57}Fe). The magnitude of f depends on the energy of the γ-ray, the mass of the atom, the nature of the crystal lattice in which the atom is bound, and on temperature.

The line energies observed in the Mössbauer spectrum are determined by three types of electronic effects on the nuclear energy levels, collectively called the hyperfine effects. These effects are the isomer shift, quadrupole splitting, and the magnetic hyperfine field.

The isomer shift arises from the interaction energy of the electrons within the nuclear volume (s electrons) with the nuclear charge. It is a measure of the electron density at the nucleus and can be used to identify the valence state of the atom under investigation.

A second hyperfine effect to be considered is the quadrupole splitting, E_Q, which is caused by the coupling of the nuclear quadrupole moment, Q, with the electric field gradient, EFG. This coupling results from the fact that the iron nucleus is not necessarily spherical but possibly ellipsoidal in shape.

The final effect which may be observed is the magnetic hyperfine effect. The presence of a magnetic field, either internal or external, will remove

the degeneracy of the magnetic sublevels of the nucleus leading to a multipeaked spectrum. The energy of each sublevel is:

$$E = -\mu H_{\text{eff}} m_{\text{I}}/I,$$

where μ is the nuclear magnetic dipole moment, H_{eff} is the magnetic field, m_{I} is the nuclear magnetic quantum number, and I is the nuclear spin quantum number. The transitions are governed by the selections rules $m = 0, \pm 1$ and energy difference between the levels is proportional to the magnitude of the magnetic field. The effective field at the nucleus, H_{eff}, may be determined from the ratio of the splitting of peaks in an unknown to splitting of peaks in a standard material having a known magnetic field. The relative intensities of the transitions in a powder having no preferred orientation of H_{eff} with respect to the incoming γ-ray are 3:2:1:1:2:3.

Mössbauer spectroscopy has been used to study the type of magnetic coupling in a material (ferro- or antiferromagnetic), to determine magnetic transition temperatures, and to investigate long range magnetic coupling in dilute alloys.[50] It has also been used extensively to study fine particle ferromagnets as is discussed below.

As may be expected, the Mössbauer spectra of fine powders of magnetic materials are often quite different than those of the bulk material. Two important parameters which change with size are the recoil-free fraction and the effective hyperfine field.

The mean-squared displacement of the Mössbauer nuclei, in part, determines whether or not a recoilless absorption will occur. The lattice in which the nuclei is bound will affect the magnitude of $\langle x^2 \rangle$, that is, the better the lattice is able to absorb the recoil energy of the atom, the smaller $\langle x^2 \rangle$ will be. A measure of the rigidity of the lattice is the Debye temperature, θ_{D}, and a higher θ_{D} indicates a more rigid lattice.[48] The importance of θ_{D} with respect to absorption area has to be considered for fine particle systems.

Von Eynatten and Bömmel studied loosely dispersed particles and particles embedded in different matrices in an attempt to understand how the magnitude of f changes with particle size.[51] They found that f, and therefore absorption area, was smaller in the dispersed particles and they attributed this decrease to either random motion of the particles or to softened surface phonons.

Qui and coworkers, continued this investigation in their work involving fine iron particles.[28] Loosely dispersed samples and samples pressed in a boron nitride matrix were prepared. At 4.2 K, both samples gave almost equal absorption areas. At 300 K, the areas were quite different, being larger for the pressed particles. Because of this difference, the authors proposed that whole particle motion played an important role in the decrease in f for the small particles.

In the same work, oxide coated iron particles were also studied. For pressed powders, where macroscopic motion of the particles was greatly reduced, they observed a greater change of f with temperature for the oxide layer when compared to the iron core. The effect remained even when the different Debye temperatures of the bulk iron and iron oxide were considered. This was taken as evidence that the phonons at the oxide surface were softened relative to the iron core and the magnitude of f was reduced for atoms in the oxide layer.

In related work, Picone and coworkers also found that oxide coated iron particles exhibited a reduced Debye temperature for the oxide layer with the iron core showing essentially the bulk value.[27] They also reported that binders such as benzophenone or paraffin increased recoilless events in a sample of iron oxide 38 nm in size by 79 and 64%, respectively.

If quantitative measurements are made on the basis of Mössbauer spectra the differences in f factors for different materials or for iron atoms in different valence states within the same material must be taken into consideration. And, as shown above, the change in f with temperature for fine particles is also important. Collins has developed a method for obtaining quantitative results which makes use of the change in f, as a result of change in $\langle x^2 \rangle$, for all materials.[52] This method necessitates the one time collection of spectra from roughly 10–100 K for the material of interest. From these data, a value of $\langle x^2 \rangle$ at 0 K is determined and it is this value which is used for all quantitative calculations.

Mössbauer spectra for particles less that 100 Å in diameter that have not been imbedded in a rigid matrix have been reported.[53] This is surprising when one considers that theoretical calculations based on the mass of the ^{57}Fe atom and the energy of the γ-ray have put a lower limit on particle size of 25 nm below which recoilless absorption should not occur.[54] In some instances, it is probable that particle interaction is occurring thereby increasing the effective mass. It has been postulated that van der Waals forces, magnetic interactions, or interstitial water, in the case of aqueous precipitates, may be responsible for small particle agglomeration.[55]

For single domain ferromagnetic particles demagnetizing fields, caused by poles of the magnetization vector at the surface of the particle,[46] and thermal excitations of the magnetization can have a pronounced effect on the observed hyperfine field.[56]

For fine particles of α-Fe, the former serves to increase the hyperfine field while the latter acts to decrease it. Because these effects are in opposition to each other, hyperfine fields at room temperature may be slightly lower or equal to that of bulk iron. However, if the spectrum is collected at a reduced temperature, where thermal excitations are nearly absent, an enhanced hyperfine field may be observed.

Niemantsverdriet and coworkers, reported a magnetic hyperfine field of 345 ± 3 kOe at 4 K for supported iron particles having an estimated size of 2 nm.[46] This was significantly larger than the bulk value of 338 kOe at 4 K. This increase was attributed to the presence of demagnetizing fields which are expected to have a magnitude of about 7 kOe for spherical, single domain iron particles. In metallic iron, the magnetic hyperfine field is antiparallel to the particle magnetization and the demagnetization fields produced by the magnetization will serve to increase the hyperfine field. Unsupported iron particles 6.6 to 10 nm in diameter have also been reported to show enhanced hyperfine fields.[54,57]

Oxide coated iron particles have been reported to exhibit a hyperfine field value for the iron core which is the same as that for bulk iron.[27] The core size was 11.4 nm and the total particle size was 37.7 nm. The temperature at which the spectra were recorded was not reported so it was not apparent whether thermal excitations were a consideration. It is possible that the core size was large enough so that the influence of demagnetizing fields was reduced. However, the presence of the oxide coating may also have had some effect.

Significant line broadening has been observed in the hyperfine spectra of fine particle ferromagnets which have a distribution of particle sizes.[58] The size distribution leads to a distribution of magnetic hyperfine fields, as a result the lines become broader. This effect has been used as a means of deducing the size distribution with the aid of computer programs.[30,59]

The total collapse of the six line hyperfine field to a singlet has been observed in superparamagnetic samples of α-Fe.[46,60] Cooling of the sample below the blocking temperature restored the six line pattern. As the blocking temperature was approached, a broad hyperfine pattern was observed. Further cooling will lead to a distinct sextet in most systems. The broadening of the lines before their collapse is analogous to motional narrowing observed in NMR experiments.[60]

In some cases, samples which show superparamagnetic behaviour in magnetization measurements behave as stable ferromagnets in the Mössbauer experiment, for data collected at the same temperature.[61] This is only an apparent contradiction as the time scales for these two measurements are different.

The fluctuation of the magnetic moment of a superparamagnetic particle has a characteristic time, τ_N. If the time of measurement is long enough, thermal equilibrium will be reached and superparamagnetic behaviour will be observed. Since the times of measurement for static magnetic measurements (a few seconds) and Mössbauer experiments (10^{-8} sec) are quite different, powders are expected to behave differently when examined by these two techniques. Some paramagnetic materials have been reported to give magnetically split Mössbauer spectra corroborating the above analysis.[62] Mulay has published a review article discussing in detail the application of Mössbauer spectroscopy to superparamagnetic systems.[63]

EXPERIMENTAL

Fine particles were prepared by cocondensation of metal vapour with excess pentane, hexane or perfluorotri-n-butylamine (PFTA) at 77 K. Upon slow warming of this frozen matrix metal atom aggregation took place. As the metal clusters formed and grew, the effects of decreased mobility and solvent coordination/reaction combined to terminate particle growth. Metal atom/vapour reactors,[64] and this technique of preparation of fine particles have been described before.[65] In some cases two metals, such as Fe and Ag were covapourized. In other cases, after iron particle formation, a thiol was added to ligate and coat the particles. Details are given below.

The fine particles were isolated in two different ways. After codeposition and warmup, volatile solvents could be pumped directly to a cold trap. The reactor was put under an atmosphere of argon gas, the reaction flask removed, and the top of the reaction flask quickly covered with aluminum foil. The flask was placed in the antechamber of the inert atmosphere "drybox" which had already been pumped down and back-filled with argon. The entire reaction flask was then transferred into the inert atmosphere chamber where the product was removed.

The powders could also be collected by vacuum filtration onto a sintered glass frit. A syphon was made of Teflon tubing. An adaptor constructed of a #20 o-ring joint butt sealed to a threaded connector (Kontes #11) was used to attach the syphon to the flask top. A second adaptor consisting of a S/T 19/38 ground glass joint (outer) butt sealed to a threaded connector allowed the syphon to be attached to the frit apparatus. During the

collection process, the powders were isolated on the frit while the solvent passed through and was collected in a Schlenk tube. The frit was then placed under an atmosphere of argon gas, the syphon removed, and the top of the frit capped. The frit apparatus was taken into the drybox where the product was removed.

All powders were stored in the inert atmosphere drybox (Vacuum Atmospheres, HE Series). Samples for XRD and Mössbauer analysis were prepared in the drybox to minimize exposure to air.

Metals and solvents

Metals. Iron metal (Fischer Scientific, Certified, Mn < 0.002%) was used without further purification. Silver shot (Johnson Matthey Electronics, 1–5mm, 99.9%) was also used as received.

Solvents. Pentane and hexane were dried over anhydrous $MgSO_4$ and distilled under N_2 into volumetric Schlenk tubes. The solvents were degassed by taking them through several freeze–thaw-pump cycles.

Perfluorotributylamine (PFTA) was obtained from 3M (ICP, PCP Divisions) and was also dried over $MgSO_4$, distilled under N_2, and degassed.

Anhydrous 1-dodecanethiol (Sigma) was used as received. This liquid was transferred under argon atmosphere to a volumetric Schlenk tube via syringe. The syringe was flushed with argon gas three times prior to filling with the liquid. The thiol was degassed, using several freeze–thaw cycles, to remove O_2 and then placed under an atmosphere of argon gas.

Metal vapour codeposition

The general reaction procedure went as follows: the metal vapour reactor was first pumped down to base pressure using a mechanical pump. The pressure was then further lowered by means of a diffusion pump. The usual final pressure was in the range of 10^{-3} torr. A liquid nitrogen dewar was then placed around the reaction flask and the flask was cooled to 77 K.

At this point, the solvent Schlenk tube was opened to the showerhead and approximately 10 cm^3 of solvent was deposited on the walls of the reactor. Warm-up of the crucible basket then commenced. The voltage across the electrodes was increased gradually to avoid cracking the basket. Once the iron metal melted, the voltage was reduced slightly so as to obtain a slow, even evaporation rate. Solvent and iron metal vapours were co-condensed on the walls of the reactor for a period of about 1 h.

After the deposition process was complete, the liquid nitrogen dewar was removed and the matrix was allowed to melt. During this warm-up, the iron atoms and small clusters, which were stable in the frozen matrix, grow to form larger particles. Once the matrix was completely melted (about 1 h) the reaction flask was backfilled with argon gas. The nanoscale powders were then ready to be isolated as described earlier.

Co-evaporation of two metals

To allow for the evaporation of two metals a double electrode reactor was constructed. It was possible to position two electrodes through each of the S/T 24/40 joints on the flask top by using universal double offset adaptors (Kontes S/T 24/25) in place of the S/T 24/40 stainless steel joints in the original design. Vacuum tight construction was achieved through use of compression caps fitted with o-rings.

This double electrode reactor was used to prepare Fe/Ag mixed metal powders. Typically, silver evaporation was started first and the evaporation of the iron started 5–10 min later. Both silver and iron vapours were condensed with pentane vapour during the course of the experiment.

Heat treatment of powders

It was sometimes of interest to subject these powders to various heat treatment procedures. The cell equipment was small enough to be taken into the drybox, loaded with a sample, and brought out into the lab without exposure of these air sensitive materials.

The heat treatment cell was constructed from a direct seal quartz to borosilicate tube (Kontes, i.d. 7mm) which was closed at the quartz end after purchase. The top and bottom parts of the heat treatment apparatus were connected by means of a ball and socket joint. The top of the apparatus was equipped with two vacuum tight stopcocks which made it possible to have either static or flowing gas atmospheres in the tube during the heat treatment process. Finally, a S/T 14/35 ground glass joint sealed with a rubber septum was used to introduce the thermocouple into the tube.

The quartz portion of the treatment tube was wrapped with electrical heating tape (Barnstead/Thermolyne, Heavy Insulated Samox.) Both the heating tape and the thermocouple were connected to a homemade temperature controller. The tip of the thermocouple was positioned approximately 2–3mm above the top surface of the sample to be heated.

The entire system was placed under a head of argon gas as well as being open to a mercury bubbler. The sample was then heated to the chosen temperature and was held at this temperature for a period of 2 h. After the heat treatment was complete, the sample was cooled and either removed to the drybox or exposed to air depending on the choice of experimental conditions.

Surface area analysis

The Brunauer–Emmett–Teller (BET) single point method was used to determine the surface areas of fresh and heat treated powders. The detailed theory behind this technique has been described in the literature.[66] The BET method involves the adsorption of a monolayer of N_2 onto the surface of the powders. Knowledge of the amount of N_2 adsorbed, the area occupied by one molecule of N_2, and the mass of the sample allowed calculation of the surface area.

To estimate the particle size, it was assumed that the particles were spherical and that the density of the particles was that of bulk α-Fe. By combining the equation which describes the surface area of a sphere with the equation which describes the density of a solid, the following relation was obtained:

$$D = \frac{6 \times 10^7}{S \times d},$$

where D was the diameter of the particles (nm), S was the surface area (cm^2g^{-1}), and d was the density of bulk α-Fe. This equation was used for the calculation of particles from BET data.

The surface area measurements were made on a Micromeritics Flowsorb II 2300 equipped with a 840 Side = TRAK mass flow controller. The absorbate gas was a mixture of 8 mol% N_2 and 92 mol% He and all absorption measurements were carried out at 77 K. Samples were degassed at 130°C for 15 min prior to N_2 absorption to remove adsorbed surface species.

X-ray diffraction

X-ray diffraction patterns were obtained using a powder diffractometer (Scintag). The source of the X-rays was Cu-K_α radiation ($\lambda = 1.541$ Å.) A p-type, high purity Ge detector was used to detect the scattered X-rays.

XRD spectra can also be used to estimate crystallite size for nanoscale materials by measuring the line broadening of the diffracted X-ray beam. All diffraction peaks have finite breadth due to the Heisenberg uncertainty principle as well as to the focusing ability of the instrument. For small particles of thickness 5–50 nm, there is an additional contribution to line broadening. This results from the lower number of crystal planes which are present in these small particles relative to the thousands of planes which make up the crystals of the bulk material.

The most widely used equation for calculating the thickness of small crystals is the Scherrer formula:

$$t = \frac{0.9\lambda}{B\cos\theta_B},$$

where t = thickness of the crystal (Å), λ = wavelength of the source X-ray (Å), θ_B = the Bragg angle and B = the half width at half maximum of the diffraction peak (rad.). For crystals in the size range 50–500 Å, it is best to use lower angle peaks for this calculation.

The above equation was used in all calculations of crystallite size. These average values were compared with average particle size calculated for these powders using transmission electron microscopy (TEM) and from BET measurements.

Air sensitive powders were prepared for X-ray diffraction analysis in the inert atmosphere box. These powders were coated with a thin layer of mineral oil to inhibit oxidation during the time needed for collection of the spectra.

Magnetic measurements

Two instruments were employed to investigate the magnetic behaviour of the fine powders. A SQUID magnetometer was used to study the behaviour of the samples from room temperature to 10 K while a vibrating sample magnetometer (VSM) was used to determine the high temperature magnetic behaviour of these materials.

A sample of known mass was sealed in Ta foil for use in the VSM experiment. The sample was then inserted in a sample rod and placed between the poles of an electromagnet. An electromechanical driver (Vibrator Model #V203, Ling Dynamic Systems) powered by a power oscillator (LDS Model TPO 50) was used to vibrate the sample in the presence of an applied field. This process induced an EMF in the pick up coils which surrounded the sample. A reference moment was produced by applying a DC current through a reference coil mounted on the upper part of the sample rod. The reference and sample signals were amplified (EG&G Model 5101 Lock-in amplifier) before the signals were passed through a divider circuit. The output of the divider circuit was proportional to the sample magnetization.

Samples for SQUID analysis were weighed then sealed with wax in quartz tubing. All samples which

had not been exposed to air were sealed under inert atmosphere conditions.

Mössbauer spectroscopy

Mössbauer spectra were collected on a Ranger Scientific Mössbauer spectrometer Model MS-1200. This unit was designed for use with an IBM PC. The multichannel analyser and Mössbauer control circuits were combined into a single unit. Data were transferred to a PC where they were fit using Mössfit software supplied by Ranger Scientific.

The spectrometer was operated in a constant acceleration mode with the 25 miCu ^{57}Co source being driven by a constant acceleration transducer (Model VT-1200). The unit was equipped with a laser interferometer which measured the triangle waveform produced by the transducer. The computer adjusted the waveform to obtain optimum linearity and stability. Non-linearity is reported to be less than 0.02% when the unit is operated within the range of ± 0.1 mm s^{-1} to ± 10 mm s^{-1} and velocity reproducibility is reported to be $\pm 0.01\%$.

A proportional counter detector (Model #PA-1200, Ranger Scientific) with Kr-CO_2 fill gas was used to detect the 14.4 keV γ-rays emitted from the sample. The experimental spectra were fit to a Lorenztian lineshape by a linear least squares fitting program.

Low temperature spectra were obtained using a liquid nitrogen cooled cryostat (Model 8CC Variable Temperature Optical Cryostat, Cryo Industries). The cryostat was pumped down to a base pressure of approximately 50 microns Hg using a mechanical pump. It was filled with liquid nitrogen and the sample was allowed to cool for 1 h prior to data collection. Helium gas, at a pressure of approximately 100 microns Hg, was used as the exchange gas.

The sample cell was constructed of aluminum metal and the windows were cut from polyethylene transparency sheets.[67] Typically 10–20 mg of sample was placed in the cell for routine measurements. The cell was loaded in the drybox and the sample pre-coated with a small amount of mineral oil. The sample cell was then placed in the cryostat under a head of helium gas to minimize exposure to air during room temperature measurements.

RESULTS AND DISCUSSION

Iron/hexane and iron/pentane systems

In a typical reaction, 0.8g of iron was co-condensed with 75cm^3 of hexane which gave a Fe : hexane molar ratio of approximately 1 : 40 in the deposited matrix. To obtain a mole ratio of 1 : 200 Fe : hexane, 0.2g of iron was deposited with 90cm^3 of hexane. Powders which were prepared in pentane required depositing 0.8g of iron with 66 ml of pentane.

The products from these reactions were isolated on a sintered glass frit. Samples were manipulated in the drybox for XRD, Mössbauer, and SQUID investigations.

The X-ray diffraction (XRD) spectrum obtained for the iron : pentane sample was similar to that of the iron : hexane powder. This sample gave a spectrum with a broad diffraction peak centred about $2\theta = 42°$ (α-Fe) which allowed estimation of the average crystallite size. Using the Scherrer equation, the average crystallite size calculated was 5 nm.

Use of the BET technique allowed estimation of the average particle size in these samples. Typical surface areas for these powders ranged from 100 (pentane sample) to 120 m^2g^{-1} (hexane sample). From these values, the average diameter of the particles were calculated and were found to be 7.6 and 6.3 nm, respectively, assuming spherical particle shape.

From transmission electron micrographs there is evidence that the particles are made up of small crystallites which are loosely held together by an amorphous layer. The crystallites appear as small bright spots in the photographic negative and are surrounded by grey coloured areas which have no distinct structure. It is likely that this material consists of solvent and/or solvent fragments which become incorporated into the powders during the warm-up process.

It was also possible to observe a chain-like structure in TEM micrographs when the sample was well dispersed. This chaining can influence the magnetic properties of the powders.[68]

The room temperature Mössbauer spectrum (Fig. 2) exhibited a distorted, broad doublet, and could be fit to a singlet ($\delta = +0.07$mm s^{-1}) and a doublet ($\delta = +0.26$mm s^{-1}, $\Delta E_Q = +0.82$mm s^{-1}). The singlet is assigned to superparamagnetic α-Fe.[69] Assignment of the doublet is more difficult. Fine particles of ferromagnetic and antiferromagnetic iron oxides are known to give doublets when behaving superparamagnetically.[69] The magnitude of δ and ΔE_Q are typical for Fe^{3+} compounds and similar values have been reported for supported and thin film α-Fe_2O_3.[70,71]

The spectrum collected at 77 K exhibited hyperfine splitting for both α-Fe and the iron oxide species. The emergence of the sextets indicates the superparamagnetic particles have been cooled below T_B but the broadness of the individual peaks

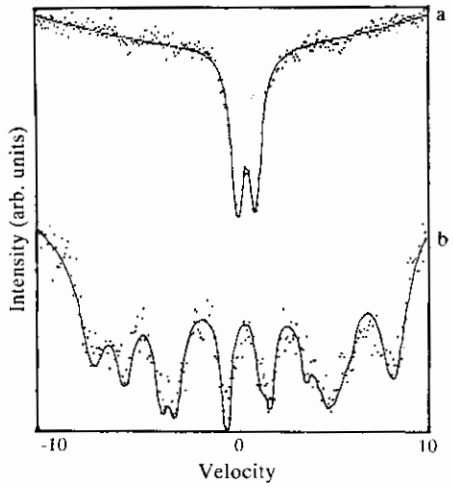

Fig. 2. Mössbauer spectra of fresh nanoscale α-Fe particles derived from Fe vapour/hexane (1 : 40) matrices. (a) Spectrum obtained at 300 K ; (b) at 77 K.

suggests that motional narrowing of the peaks is not complete. There is also overlap of some peaks from the two sextets. Hyperfine fields have been roughly estimated from the splitting of the outermost lines for both species and were found to be 344 kOe and 460 kOe for the α-Fe and iron oxide, respectively. The value for α-Fe is typical for fine particles since hyperfine fields larger than bulk are often observed.[72] On the other hand, the hyperfine field of the iron oxide species is much lower than that of bulk α-Fe_2O_3 (H_{eff} = 535 at 4 K). However, it should be noted that the Mössbauer spectra of thin films 50 nm in thickness of amorphous α-Fe_2O_3 showed reduced H_{eff}[73] ; for these films H_{eff} was found to be 460 kOe and 490 kOe for films deposited at substrate temperatures of 20 and 60°C, respectively. The surface atoms of fine α-Fe_2O_3 are known to have reduced hyperfine fields, and the combination of fields produced by surface and bulk atoms leads to broadened Mössbauer lines.[74] In addition, fine particles of iron carbides have smaller hyperfine fields ranging from 170–220 kOe.[75] From these considerations, the doublet observed for our sample for the room temperature Mössbauer spectrum is assigned to iron oxide, most probably α-Fe_2O_3.

Iron/pentane powders gave similar Mössbauer spectra. It was only possible to obtain low temperature spectra exhibiting only iron metal peaks for one of these samples when *stringent* conditions were employed to prevent accidental oxidation of the sample.

Magnetic properties

The data for Fe/hexane powders are summarized in Table 1. The samples exhibited relatively small coercivities at room temperature and for each sample the coercivity increased as the temperature decreased.

Note that the M_s values are much smaller than expected for bulk α-Fe (220 EMU g^{-1}). Also, their parameters were affected by the Fe : hexane deposition ratio, especially when the ratio was higher than 1 : 250. It has been shown that higher dilution leads to smaller metal crystallites, due to complex growth phenomena in cold matrices.[76] So larger crystallites in the 1 : 40 ratio experiments exhibit slightly higher M_s values, and these results support earlier reports of lower M_s values for smaller particles.[77] On the other hand, our Mössbauer data indicate the presence of some iron oxides (due to scavenging of adventitious oxygen in spite of careful handling under argon). Thus, the smaller M_s values might also be attributed to the presence of these oxides. For comparison we note that literature values for bulk samples are : α-Fe (220 EMU g^{-1}), Fe_3O_4(92), α-Fe_2O_3 (0.6), γ-Fe_2O_3 (76) all at 300 K.[68]

SQUID magnetometry data indicated that these samples were superparamagnetic down to at least 220 K ; that is magnetization (M) plotted against H/T for data collected at 220 K and 300 K showed superimposable lines. Below 220 K hysteresis was

Table 1. Average values of saturation magnetization M_s and coercivity H_c for fresh nanoscale α-Fe particles derived from Fe vapour/hexane. Surface oxide is present

Fe : hexane molar ratio	matrix M_s (EMU/g^{-1} of sample)	H_c (O_e)
1 : 40	90	750 (10 K) 10 (300 K)
1 : 250	50	840(10 K) 30 (300 K)

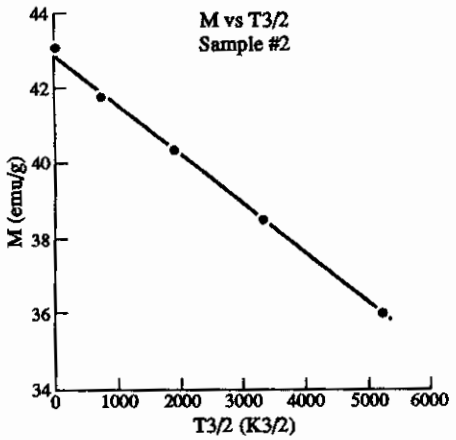

Fig. 3. M vs $T^{3/2}$ for Fe nanoscale particles derived from an Fe : hexane matrix ratio of 1 : 250.

observed, however, indicating that ferromagnetism was setting in.

Saturation magnetization values could be fit to the Bloch $T^{3/2}$ law. Figure 3 shows such a plot from which an estimated Bloch constant, B, of value of $3.0 \times 10^{-5}K^{3/2}$ was derived. Similar plots for several samples allowed estimation of B for these powders which ranged from 1.4 to 3.5×10^{-5}. All values are considerably larger than the bulk value of $3.3 \times 10^{-6}K^{3/2}$. This behaviour has been observed for oxide coated α-Fe particles having diameters of 15–40 nm, where B values ranging from 4.87×10^{-6} to $6.30 \times 10^{-6}K^{3/2}$ were reported with the smaller particles having the larger value.[78] This effect was explained qualitatively in terms of surface magnetic effects whereby softening of the surface phonons leads to a greater temperature dependence of the magnetization of the fine particles. Particles of Fe_3O_4 coated α-Fe having diameters of 2.5–13.0 nm were reported to have B values ranging from 2.5×10^{-5} to $6.0 \times 10^{-6}K^{3/2}$, respectively.[29] The values reported here are in good agreement with these previous studies.

The iron/pfta system

Introduction. The use of non-polar alkane solvents for preparation of fine powders of α-Fe resulted in products which were easily oxidized and which contained some carbonaceous material. We considered that co-depositing iron atoms with a more inert solvent might allow the growth of iron fine particles with less incorporation of solvent and/or solvent fragments into the final product. Xenon was considered as one alternative. However, earlier results showed that very large crystallites were produced, too large to have unusual catalytic or magnetic properties.[65b] Likewise, perfluoroalkanes were also considered, but here again the particles/crystallites obtained were too large.[65b]

During the same time period, studies had been completed on the use of perfluorotri-n-butylamine (PFTA) as a solvent for metal vapour preparation of Au fine particles.[23a] These powders were unique in that they could be dried and then suspended in other organic solvents such as acetone or ethanol. The individual particles in these colloids were less susceptible to agglomeration than particles prepared in ethanol or acetone alone. These results seemed to indicate that the PFTA was coordinated to the surface of the gold particles resulting in their unusual solubilities and resistance to agglomeration.

These results prompted us to investigate the preparation of iron fine powders in PFTA. We hoped that the particles prepared in PFTA would also have a fluoroorganic coating and that this surface layer would serve to protect the particles from oxidation. Because this solvent is described as inert, indeed its commercial name is "fluoroinert",[79] we thought that the iron atoms and/or clusters might show little reactivity towards PFTA during particle growth. This system did not behave as we had hoped. Instead, the iron atoms were very reactive resulting in the cleavage of C—F bonds of the solvent and in the formation of mixed iron fluoride and iron powders.

Nanoscale particles were prepared by co-depositing Fe : PFTA ratios of 1 : 25 to 1 : 40. After warm up from 77 K to 300 K the fine powder was isolated and XRD spectra obtained. A representative spectrum is shown in Fig. 4.

The strongest peaks in these spectra are assigned to FeF_2 and γ-Fe_2O_3. There are also weak peaks for α-Fe. The crystallite size calculated from this

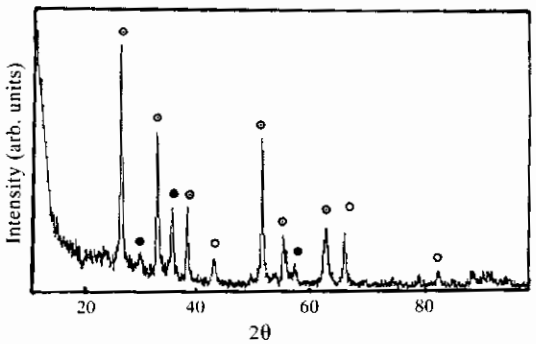

Fig. 4. XRD spectrum of nanoscale Fe particles derived from an Fe : PFTA ratio of 1 : 25. ○ Fe, ⊙ FeF_2, ● γ-Fe_2O_3.

spectrum for α-Fe was less than 5 nm. Heat treatment at 400°C for 2 h under argon yielded a spectrum where strong peaks were observed for FeF_2 and very weak peaks for α-Fe. Some peaks for γ-Fe_2O_3 are present and are weaker than in the spectrum of the fresh sample. The crystallite size calculated for FeF_2 was 14 nm.

The average surface area of the fresh powders was found to be 125 m^2g^{-1} using BET N_2 absorption measurements. The particle size calculated using this value for surface area was 6 nm assuming spherical particle shape and that the density of the powder was 7.86 g cm^{-3}.

The TEM photographic negatives indicated that small particles 10 nm or less in diameter were the building blocks for larger particles having sizes 100 nm or greater. As in the Fe/hexane system the particles appeared to be connected through a layer of amorphous material. The average particle size estimated from these photographs was 16 nm. Higher magnifications, which would allow the sizing of particles less than 10 nm in diameter, gave blurry images which were not suitable for particle size estimation. Therefore, the above estimate of 16 nm may be somewhat high.

XPS, SIMS and auger analysis. Figure 5 exhibits XPS spectra collected for an Fe/PFTA fine powder. The $Fe_{2p3/2}$ region of the spectrum showed one peak at 717 eV. This is consistent with the value of 716 eV reported by Veremeyenko and coworkers, for FeF_3 thin films on iron.[80] These workers reported a layered structure of iron fluoride on iron with FeF_3 occurring at the air interface and FeF_2 at the Fe substrate interface. There were no other peaks observed in this region of the spectrum.

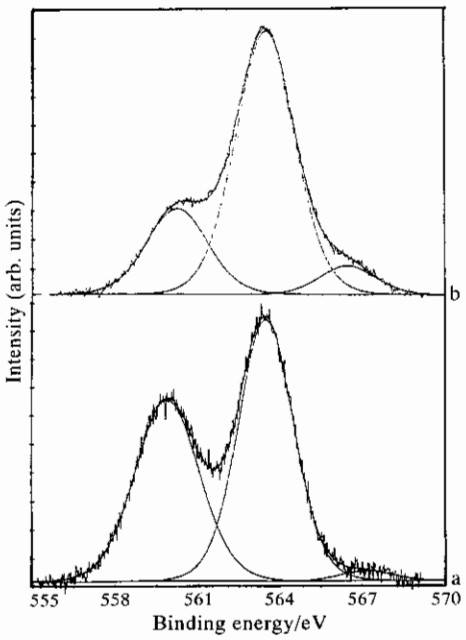

Fig. 5. XPS spectra for nanoscale $Fe/FeF_2/FeF_3$ particles obtained from Fe:PFTA codepositions. (a) fresh; (b) after 30 h in the instrument.

For our sample, two peaks were observed in the F_{1s} region of the spectrum occurring at 692 and 688 eV. After 10 h in the instrument, the peak at 692 eV decreased in intensity while a third peak at 685 eV emerged. The higher binding energy peak was observed to decrease further in intensity after 30 h in the instrument while the intensity of the peak at 685 eV remained the same. Etching of the sample for 3 min (Ar^+ ions, 5 kV, 3 mA) caused the peak at 692 eV to decrease substantially in intensity. At the same time, the peak at 685 eV became more prominent.

The peak at 685 eV is consistent with the F_{1s} peaks observed in transition metal fluorides. For example, the binding energy in NiF_2 is 684.6–685.2 eV.[81] The higher energy peaks are similar to that observed in CF_2 containing polymers, $(CF_2)_n$: 688.9–689.5 eV, and fluorinated graphite, CF: 689.3–689.9 eV, C_4F: 687.0–687.5 eV.[81]

The changes in the intensities of the F_{1s} peaks were accompanied by a decrease in the peak intensities of the C_{1s} occurring at higher binding energies. Absolute energies for the five C_{1s} peaks observed in the spectrum could not be exactly determined due to the limitations of the fitting program but were estimated to occur at binding energies 284.6, 287.2, 288.2, 289.8 and 294 eV. The peak at 284.6 eV is consistent with graphitic carbon. This peak was also observed in the spectrum of the indium foil used as a sample holder. The peaks at higher energy (~294 and 289.8 eV) are near the same energy as the C_{1s} peaks observed for fluorine containing polymers $(CF)_n$: 291.8 eV, $[CF(CF_3)CF_2O]_n$: 291.4, 293.2, 293.8 eV, and cyclic fluoroorganics: C_6F_6: 288.4 eV.

The appearance of a C_{1s} peak at 293 eV in NiF_2 and FeF_2 thin films on Ni and Fe is similar to that observed in our samples.[40] In addition to the C_{1s} peak shifted by 7 eV, a shift in the F_{1s} peak to 689 eV was also observed in these films. Treatment of the films up to 500°C caused the gradual, simultaneous disappearance of both the shifted F_{1s} and the high energy C_{1s} peak. The shift in the binding energy of the F_{1s} peak was attributed to the formation of a compound with carbon.

Positive SIMS using Ar^+ ions (2 kV, 10 mA) showed peaks for F, CF_2^+, and FeO for our samples. No peaks occurred at greater than 73 Da in the spectrum. Negative SIMS analysis showed peaks corresponding to F^- and F_2^-. In this

spectrum, no peaks at greater than 40 Da were observed.

Auger analysis indicated that the fluorine peaks occurred at higher kinetic energy when compared to F^- in ionic compounds, i.e. LiF.[81] In the fresh sample, three fluorine peaks were observed at 612 (F1), 656 (F2), and 633 eV, and the ratio of F(2)/F(1) was 12. After sputtering, this ratio decreased to 2. The carbon peak occurred at 272 eV indicating that the carbon was not carbidic. Finally, no peak was observed at 703 eV which would correspond to Fe.

A summary of these data is as follows. There is a reaction of the growing iron clusters with solvent which leads to the formation of FeF_2. However, some oxidation of the FeF_2 on the surface of the particle occurs forming FeF_3 as observed by the $Fe_{2p3/2}$ peak at 717 eV. There remain some $-CF_x$ ($x = 1$–3) fragments, especially on the surface of the powders from the PFTA solvent. As the surface of the particles is removed, the higher binding energy C_{1s} and F_{1s} peaks decrease in intensity indicating the loss of $-F$ and/or $-CF_x$ fragments. It is possible that the F_{1s} peak observed at 685 eV, which showed an increase in intensity after aging the sample in the instrument and after etching the surface, corresponds to FeF_2. This assignment is supported by XRD which indicate a fraction of the powder is FeF_2. No evidence was found for the presence of Fe(0) from XPS, SIMS, or Auger data, although XRD did show the presence of α-Fe. We conclude that a core-shell structure of Fe)FeF_2)C_xF_y) was formed, with FeF_2 as the major component.

Mössbauer spectra. Mössbauer spectra were collected at room temperature for several different samples with various matrix molar ratios Fe : PFTA. All spectra could be fit to three sets of doublets. The values of δ and ΔE_Q obtained from these fits were compared with the data of Ramasamy and coworkers, who prepared nanocrystalline FeF_2.[82] Agreement was very good, confirming that FeF_2 was a major component in our samples. Upon exposure to the atmosphere, a slow conversion took place over several days, such that FeF_3 and/or γ-Fe_2O_3 were formed, as deduced from changes in the Mössbauer spectra and comparisons with the literature.[83,85]

Magnetic properties. The magnetic behaviour of the Fe/PFTA samples can not be described as superparamagnetic or ferromagnetic. The value of M_s for all samples ranged from 3 to 12 EMU g^{-1}, and such low values cannot be attributed to α-Fe or to γ-Fe_2O_3.

Since FeF_2 appeared to be the major component in these samples, and since FeF_2 is an antiferromagnetic material, H/M (or $1/\chi$) were plotted vs T (Fig. 6). The data could be fit to a straight line as expected for an antiferromagnetic material exhibiting Curie–Weiss behaviour.[8] However, no minimum in the plot was observed which would indicate the transition through the Neel temperature of the material under investigation.

Since data were collected down to 10 K, and the literature value for the Neel temperature of FeF_2 is 78 K,[8] it might be expected that the plot of $1/\chi$ vs T for our sample should begin to rise again after cooling the sample to below 78 K. From our data it appears as though T_N for our fresh powders must lie below 10 K.

The reduction of T_N for fine particle antiferromagnets has been reported in the literature. Amorphous α-Fe_2O_3 thin films 50 nm in thickness exhibited Neel temperatures of 48 and 62 K for samples deposited on substrate temperatures of 20 and 60°C, respectively.[85] The Neel temperature for bulk, crystalline α-Fe_2O_3 is 950°C.[8] Similarly, amorphous powders of FeF_3 had an average T_N of 28 K whereas the literature value for the bulk material is 363 K.[83]

The point at which $1/\chi$ vs T intercepts the x-axis gives the Curie constant, θ_c. For antiferromagnetic materials the straight line will intercept at negative values of T.[8] Reduced values of θ_c also have been observed in the thin films of α-Fe_2O_3 discussed earlier. The literature value for the bulk oxide is 200 K but the thin films had $\theta_c = 90$ K, estimated from their plot of $1/\chi$ vs T.[8] Amorphous FeF_3 exhibited a θ_c of 486 K as compared to the bulk value of 610.[83] The average value of θ_c observed for three of our samples was 83 K as compared to the literature value of 117 K for bulk crystalline FeF_2.[8]

We can conclude that during the codeposition of iron atom and PFTA vapours at 77 K, extensive

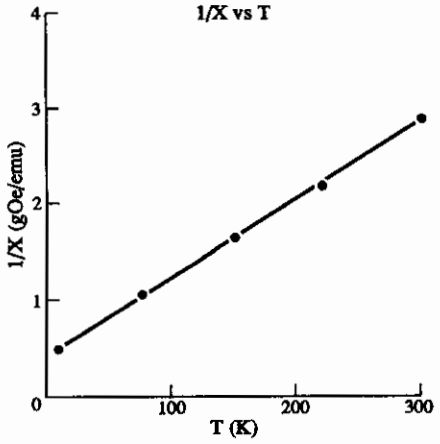

Fig. 6. Plot of $1/\chi$ vs T Fe/PFTA derived samples, mainly composed of FeF_2.

reaction takes place, and ultrafine FeF_2 is formed as the main component. These FeF_2 powders possess magnetic properties similar to other antiferromagnetic fine powders such as Fe_2O_3[85] and FeF_3.[83] While the change in magnetization with temperature of these powders could be fit to the $1/\chi$ vs T law expected for antiferromagnetic materials, reduced Neel temperatures (T_N) and Curie constants (θ_c) were observed. Heat treatment of the fresh powders at 400°C, in the presence of argon gas, resulted in the partial conversion of FeF_2 to the less common HTB phase of FeF_3.[85] These observations provide further evidence for the unique behaviour of nanoscale materials.

The FeF_2 is easily oxidized in the presence of atmospheric moisture and oxygen to FeF_3 and $FeF_3{\cdot}H_2O$. Some amount of γ-Fe_2O_3 was also present in the powders. The oxidation process may be written as:

$$12\,FeF_2 + 3O_2 \rightarrow 8FeF_3 + 2Fe_2O_3, \qquad (1)$$

$$8FeF_3 + 8H_2O \rightarrow 8FeF_3{\cdot}H_2O. \qquad (2)$$

Although written separately, the hydration and oxidation processes may take place concommitantly. Overall, the behaviour of these powders with respect to aging and to oxidation is analogous to that observed during the formation of thin films of FeF_2 on iron.[80,87,88]

Iron/silver bimetallic fine powders

One of the unique aspects of the metal vapour–solvent co-deposition technique is the ability to deposit two different metals into the freezing matrix. This allows for the formation of many interesting bimetallic powders. In the past, this method has been used to prepare Pt–Sn,[89] Au–Sn,[23e] Fe–Co,[23f] and Pt–Fe[23d] mixed metal clusters.

A recent investigation into the preparation of bimetallic powders of immiscible metals using this approach has yielded unusual products.[90] In this study, iron atom and lithium atom vapours were co-deposited into freezing pentane. As the mixed metal matrix was allowed to warm to room temperature, atom agglomeration occurred and Fe–Li particles were formed with some incorporation of the fragments of the organic solvent.

Under oxidizing conditions, lithium behaved as the sacrificial metal forming lithium oxide and lithium hydroxide coated α-Fe particles. Also, by proper choice of heat treatment conditions, controlled α-Fe particle growth was achieved. Exposure of the powders to air after growth of the iron crystallites did not lead to degradation. After long exposure to air, the lithium compounds were converted to $LiCO_3$ and protection of the α-Fe core was excellent.

The success of these experiments prompted us to investigate other bimetallic systems of immiscible metals. While iron is soluble in both copper and gold, iron and silver are immiscible.[91,92,93]

It has been possible to prepare thin-film, solid solutions (i.e. alloys) of Fe in Ag using ion implantation,[94] sputtering,[95] and thermal evaporation techniques.[96] In the case of ion implantation, analysis of the samples revealed that most of the Fe containing phases were not Fe–Ag alloys even though the systems were dilute with respect to Fe ($\approx$5 atom %). Thin films prepared by rf sputtering allowed the formation of more concentrated Fe–Ag solid solutions. This technique, which is also called the vapour-quench method, relies on the rapid quenching rate of the vapour deposited atoms onto a cooled substrate. The liquid state is effectively avoided and phase separation of Fe and Ag can be reduced. The concentrated solid solutions prepared by the vapour-quench technique exhibited a single bcc phase in the Fe-rich regions and a single fcc phase in the Ag-rich regions,[97] even though Fe and Ag are immiscible. The non-equilibrium solutions are ferromagnetic and have been shown by Mössbauer spectroscopy to exhibit perpendicular magnetic anisotropy near phase boundary regions.[98] The formation of non-equilibrium phases by the vapour quench technique is influenced by several factors, including the temperature of the substrate.[99] Lower temperature favours the formation of the non-equilibrium phase since the substrate behaves as a better heat sink, accepting the heat of vapour atoms and reducing their mobility. The Fe–Ag alloys sputter deposited onto liquid nitrogen cooled substrates have larger single bcc and fcc regions when compared to alloys prepared using water cooled substrates.[100] No literature reports were found for fine powder Fe–Ag alloys.

In effect, our SMAD metal–vapour solvent codeposition technique is a version of the vapour quench technique, but rather than trapping the atoms on a cooled substrate, the atoms are trapped in frozen solvent at 77 K. Because this method allows for intimate mixing of the metals at the atomic level, we considered the possibility of isolating a metastable state of Fe–Ag in a fine powder form in gram quantities. The prospect of inducing the formation of a protective silver coating over α-Fe crystallites, analogous to the Fe–Li system, or the formation of an ordered alloy of Fe and Ag by choice of heat treatment conditions was also of interest.

The results obtained from XRD and Mössbauer spectra indicate that our Fe–Ag fine powders are similar to the thin films prepared by ion implan-

tation in that small smounts of Fe/Ag solid solutions were observed. Mössbauer spectra were particularly interesting in that the absorptions of individual iron atoms in the fcc silver matrix were observed as well as the coalescence of these atoms to form clusters during heat treatment. The influence of particle size on the magnitude of the magnetic hyperfine field was also established.

XRD spectra. Table 2 lists the silver crystallite sizes for samples with various ratios Fe : Ag. The trend is towards larger Ag crystallites with increasing concentration of Ag. It was not possible to estimate Fe crystallite sizes due to overlap of the remaining Ag peaks with the Fe diffraction peaks. One pure α-Fe peak can be observed at $2\theta = 83°$ but it is of low intensity and at a high value of 2θ. Therefore it was not suitable for crystallite size estimation according to the Scherrer equation.

All spectra of newly prepared samples showed broad diffraction lines indicating that the crystallites were small but not completely amorphous. The spectra resemble those of Sumiyama and coworkers, who reported a single bcc phase at high at% Fe (e.g. Fe : Ag, 4 : 1) and a single fcc phase at high at% Ag (e.g. Fe : Ag, 1 : 4) for sputter deposited thin films.[95a] However, the fcc phase of Ag was observed in the XRD spectra of all of our samples, even those with very low Ag concentrations, such as Fe : Ag 9 : 1. While there may be some diffusion of the Fe into the Ag phase in these powders, there is no evidence for the presence of an ordered Fe–Ag alloy in the fresh powders. We cannot rule out that some fraction of our samples is an amorphous alloy of iron and silver.

Since there was the possibility of a disordered, amorphous alloy phase in our samples, heat treatment studies were conducted at temperatures of 100, 250 and 400°C to determine if a transition to an ordered Fe–Ag alloy could be observed. Figure 7 illustrates the changes in the XRD spectrum after heat treatment under flowing argon gas for 2 h at the temperatures indicated.

As expected, Ag crystallite sizes changed with the temperature chosen for heat treatment, going from about 5 nm to 20 nm over the 25–300°C range. No evidence for the formation of an ordered Fe–Ag alloy was found in the XRD spectra for our samples after treatment at any of the temperatures studied. If such a transition had occurred, extra diffraction peaks normally not observed for a pure fcc or bcc system would be present in the XRD spectrum.[101] Also, all samples remained air sensitive after heat treatment casting doubt on the idea that a structure consisting of a protective layer of Ag over a α-Fe core had formed after heat treatment of the powders.

Mössbauer spectra. The room temperature spectra of all samples showed only doublets and singlets with no indication of a magnetically split sextet.

Table 2. Summary of XRD Ag crystallite size with varying molar ratio Fe : Ag. (About 1 g of total metal codeposited with 80 cm^3 pentane at 77 K following by warming to 300 K)

Molar ratio Fe : Ag	Ag crystallite Size (nm)
4 : 1	4.4
3 : 1	4.7
1 : 1	10.0
1 : 3	6.5
1 : 9	7.0
1 : 15	8.4
Ag Only	12.0

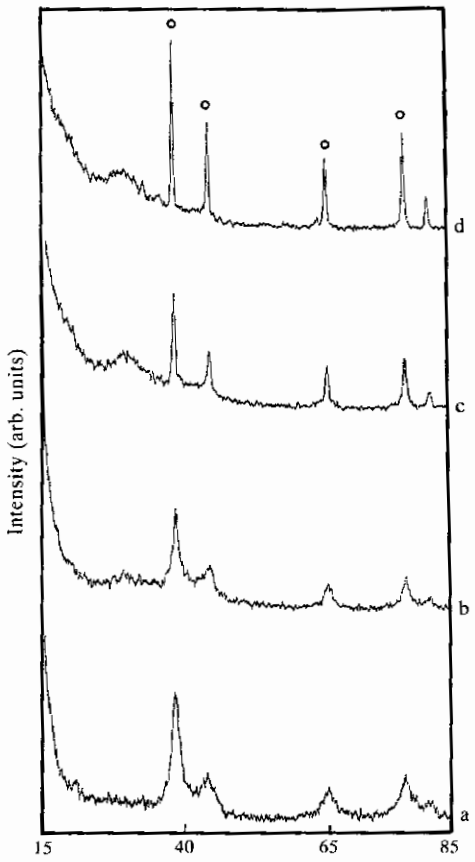

Fig. 7. Collective XRD spectra for Fe/Ag samples (a) fresh powder and after heat treatment at (b) 100, (c) 250 and (d) 400°C for 2 h under a head of argon gas. ○ = Ag.

Spectra for samples with different molar ratios Fe : Ag, could be fit to two singlets and a doublet. Table 3 lists the values of δ and ΔE_Q obtained from the computer fit for our samples.

Singlet A, which exhibited isomer shifts ranging from 0.06–0.08 mm s^{-1}, is assigned to small clusters of superparamagnetic α-Fe. The observed isomer shift for this singlet is in good agreement with that observed in other systems of nanoscale iron particles.[102]

The isomer shift values of singlet B ranged from 0.45–0.53 mm s^{-1}. These values are similar to those reported by Longworth and Jain for iron atoms having twelve silver nearest neighbour atoms, i.e. isolated iron atoms.[94] They observed singlets having isomer shifts of 0.50–0.52 mm s^{-1} for Ag foils implanted with 1×10^{15} and 2×10^{16} atoms ^{57}Fe cm^{-2}, respectively, and the per cent contribution of the atoms to the total spectral area was observed to decrease from 52 to 27% when the concentration of ^{57}Fe was decreased from 1×10^{15} to 2×10^{16} atoms cm^{-2}. The same trend was observed on our samples as can be seen from the data of Table 3.

The doublet observed in our samples was observed to have $\delta = 0.22$–0.29 mm s^{-1} and $\Delta E_Q = 0.73$–1.08 mm s^{-1}. The assignment of this doublet is difficult as it could arise from several different iron species. Therefore, a low temperature Mössbauer spectrum was obtained (Fig. 8).

The majority of the spectrum was fit to three sextets but it still contained small contributions from the singlets and doublet observed in the room temperature spectrum. Other samples gave similar low temperature spectra, however, these spectra, in general, did not have such well defined peaks. These observations indicate that there is a distribution of particle sizes in these samples with some particles small enough to behave superparamagnetically at 77 K.[103]

Table 3. Summary of Mössbauer parameters for samples having various molar ratios of Fe :Ag. Data from spectra collected at room temperature

Ratio Fe:Ag[a]	δ Iron clusters[b]	δ Iron atoms[b]	δ Iron oxide[b]	ΔE_Q Iron oxide[b]
4:1	0.06 [17]	0.45 [5]	0.29 [78]	0.89
3:1	0.06 [21]	0.49 [12]	0.24 [67]	0.96
1:1	0.06 [13]	0.45 [10]	0.22 [76]	0.73
1:3	0.08 [17]	0.47 [20]	0.25 [63]	0.89
1:9	0.06 [21]	0.53 [27]	0.25 [51]	1.08

[a]Fe and Ag codeposited with excess pentane at 77 K followed by warming to room temperature.
[b]Numbers in brackets refer to percent contribution to the total Mössbauer absorption area.

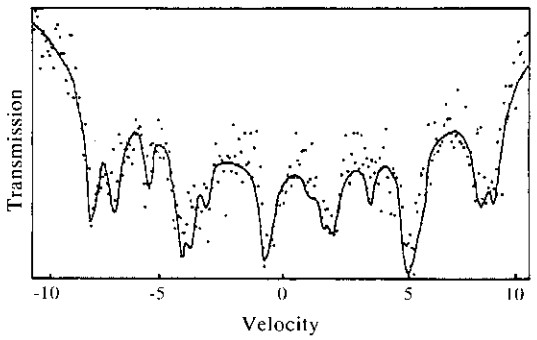

Fig. 8. Mössbauer spectra for Fe/Ag (3 : 1) collected at 77 K.

The hyperfine fields estimated from the computer fit of the spectrum shown in Fig. 8 were 344, 448, and 495 kOe for the three sextets. Since the emergence of these sextets at low temperature accompanies a decrease in the intensity of the peaks observed at room temperature., the sextets are broadly defined to be a result of cooling superparamagnetic iron containing particles below their blocking temperature.

More specifically, the sextet which has a hyperfine field of 344 kOe we assign to fine particles of α-Fe. These small particles gave rise to singlet A in the room temperature spectra. The observed hyperfine field in these clusters is larger than that for bulk α-Fe at the same temperature (≈338 kOe).[72] The observed increase in the hyperfine field of small α-Fe particles is a result of demagnetizing fields originating on the surface of the particles. Niemantsverdriet and coworkers have reported a similar hyperfine value of 345 kOe for supported, 2 nm particles of α-Fe at 4.2 K.[72] Unsupported particles 6.6–10 nm in diameter have also been reported to show enhanced hyperfine fields.[104] Although the hyperfine field for our sextet is similar in magnitude to that observed by Chien and Unruh for concentrated Fe–Ag alloys, it does not exhibit the extreme peak assymetries observed in their thin films.[95b] The sextet in our samples is therefore assigned to fine particles of α-Fe.

The sextets having hyperfine fields of 495 and 448 kOe are assigned to iron atoms located at the A and the B sites crystallographic sites, respectively, of Fe_3O_4.

We conclude that the metal vapour pentane codeposition procedure for making Fe–Ag bimetallic powders yielded mixtures of the pure Fe and Ag phases as the major crystalline products. However, there were observed in the Mössbauer spectra of all

samples absorbances due to Fe atoms isolated in a fcc Ag matrix. The concentration of these isolated atoms was observed to decrease with increasing Fe : Ag molar ratios. In addition, there was evidence from low temperature Mössbauer spectra of the presence of Ag atoms within the lattice of fine particle Fe_3O_4 which had been formed by oxidation of the fresh samples. Thus, it was possible to prepare solid solutions of Fe in Ag (and vice versa) but the systems were not homogenous.

The iron/thiol system

Whitesides and coworkers reported the formation of monolayers of alkane thiols on gold microelectrodes.[106] The ordered monolayers of the long chain thiol molecules were formed by coordination of the sulphur atom of the molecule to the gold surface. Further studies involving functionalized thiols containing ferrocenyl derivatives resulted in the formation of approximately a monolayer of the redox active ferrocene reagent on the microelectrode surface.[107]

These studies persuaded us to investigate the use of an alkane thiol to trap iron particles prepared in pentane. We saw the possibility of the coordination of the sulphur atom of the thiol molecule with the surface iron atoms of the particles to form a surface layer of organic material. The presence of this surface layer might serve to protect the particles from oxidation or might lead to particles with unique magnetic properties as was observed in the iron/oleic acid system.[6a]

The thiol chosen for these studies was 1-dodecanethiol because of its physical properties (bp = 266–283°C, density = 0.845 g ml^{-1}) and therefore its ease in handling. Powders prepared with molar ratios Fe : thiol : pentane 1 : 2 : 40 were air sensitive. However, heat treatment of the powders led to the formation of FeS coated α-Fe crystallites which were found to be air stable.

A typical experiment involved the codeposition of approximately 0.8g Fe metal with 70 cm^3 of pentane at 77 K. The frozen matrix was allowed to warm to room temperature over a period of about 1 h. At this point the reactor was filled with argon. Previously degassed 1-dodecanethiol (7 cm^3) was allowed to drip through the showerhead into the Fe/pentane slurry. The mixture was allowed to stand for approximately 10 min and then the product was vacuum filtered onto a sintered glass frit and the black solvent mixture was removed. The frit was then capped, keeping a flow of argon into the frit during the capping process. The frit was then taken into an inert atmosphere box and the product removed and stored there. All manipulations of the sample were carried in the inert atmosphere box. The black powders were observed to be pyrophoric if exposed directly to air.

Heat treatments of the fresh powders were carried out at 100, 200, 300, 400, 500 and 600°C for 2 h under a head of argon gas.

Crystallite and particle sizing. The XRD spectra for fresh samples (protected with mineral oil) and those heat treated at 100 and 200°C showed no peaks for Fe crystallites, thus indicating an amorphous nature.

Figure 9 shows the XRD spectra collected after heating a sample to (a) 400, (b) 500 and (c) 600°C. The crystalline peaks observed in this spectrum, in addition to peaks for α-Fe, are assigned to FeS (troilite). The XRD crystallite sizes for these two compounds are presented in Table 4.

Also listed in Table 4 are the particle sizes as determined by BET measurements. As expected, the trend is towards larger sizes with increasing heat treatment temperature as more sintering of the particles occurs. No BET measurements were done on the fresh samples since adsorbed thiol interferes in this measurement. The particle sizes listed for the

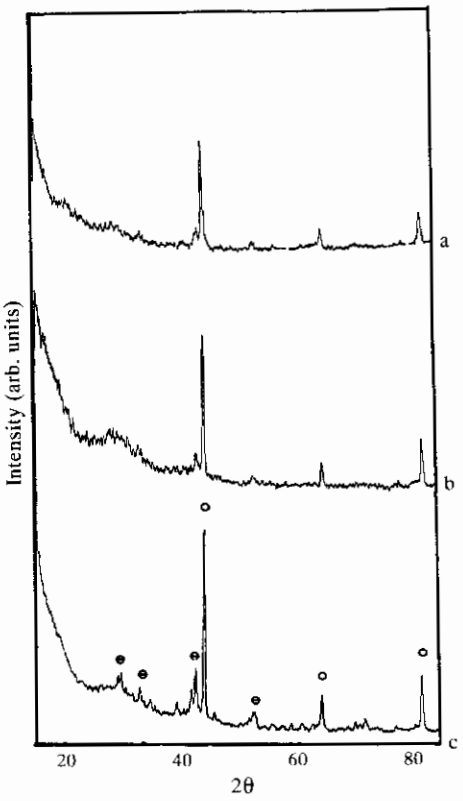

Fig. 9. XRD spectra for Fe/thiol after heat treatment at (a) 400, (b) 500 and (c) 600°C followed by exposure to air. ⊖, FeS; ○, Fe.

Table 4. Summary of BET and TEM particle sizes and XRD crystallite sizes for Fe/thiol heat treated at various temperatures

Heating Temp.(°C)	BET (nm)	XRD(nm) crystallite sizes		TEM (nm)	
		Fe	FeS	Core diameter	Shell thickness
Fresh	—	—	—	< 5	—
100	86	—	—	< 5	—
200	26	—	—	< 5	—
300	57	14	—	23	6
400	40	19	—	25	5
500	47	22	10	36	7
600	—	34	19	42	9

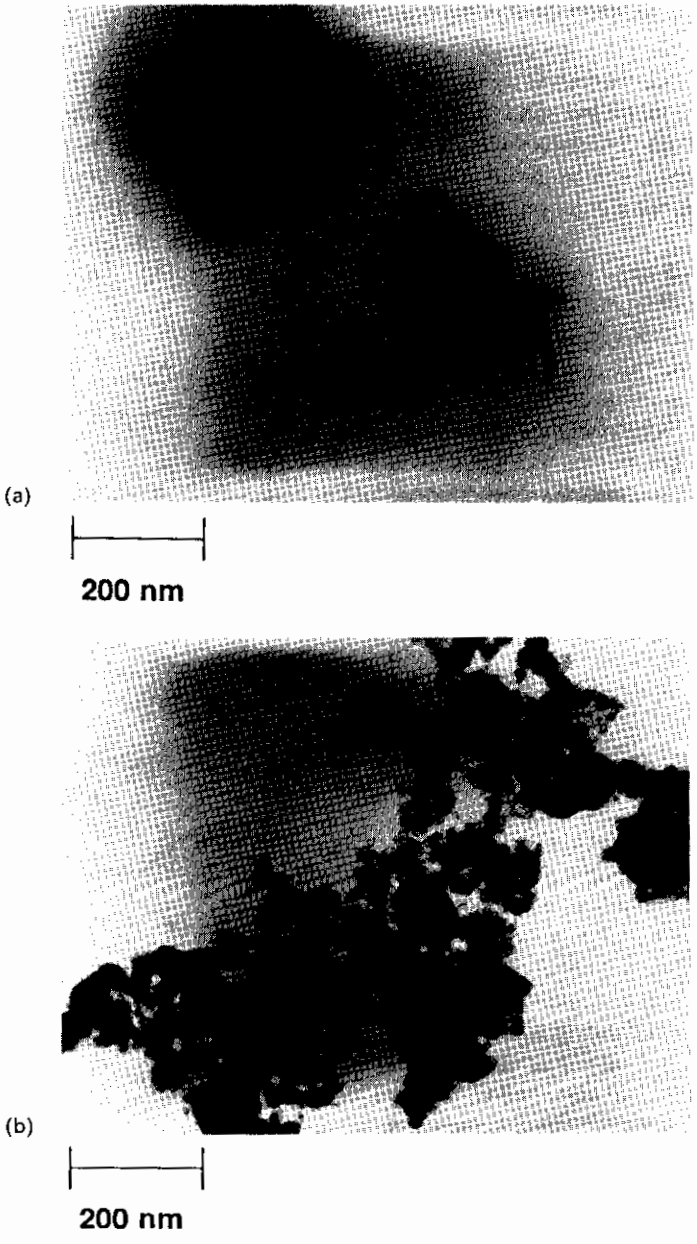

Fig. 10. TEM photographs of fresh and heat treated Fe/thiol samples, (a) fresh, (b) 300°C obtained at magnification of 92.65 K.

sample after heat treatment to 100 and 200°C may also be affected by adsorption of dodecanethiol.

Transmission electron micrographs show some very interesting changes in these particles with heat treatment. Figure 10 shows TEM photographs (magnification 92.65 K) of a sample (a) before heat treatment and (b) after heat treatment at 300°C. The sample after heat treatment consisted of small crystallites held within what appears to be an amorphous coating. The appearance of a core and shell structure for some particles is also evident (note the lighter centres and dark edges of some particles in Fig. 10b).

Mössbauer spectra. The room temperature Mössbauer spectra of the fresh and heat treated samples of Fe/Thiol are shown in Fig. 11. The spectrum before heat treatment shows a quadrupole split doublet having $\delta = 0.17$ mm s^{-1} and $\Delta E_Q = 1.04$ mm s^{-1}. These values are consistent with Fe^{3+} compounds,[108] and superparamagnetic iron oxides.[70] Because the peak towards negative velocity has a larger area, a singlet near zero velocity could also be present as a result of superparamagnetic α-Fe.[72] No change in the room temperature spectrum of this sample was observed after heat treatment to 100°C.

As the heat treatment temperature was increased the gradual emergence first of a sextet due to α-Fe and second of a sextet due to FeS was observed. The hyperfine fields observed for α-Fe (332 kOe) and FeS (313kOe) are in good agreement with the literature values of 330 kOe[109] and 312 kOe,[110] respectively, at room temperature. The spectra at room temperature show no evidence for the formation of any iron oxide compounds e.g. γ-Fe_2O_3, α-Fe_2O_3, or Fe_3O_4, all of which have much larger hyperfine fields than α-Fe.[109]

Low temperature spectra of samples heat treated at 100, 200, 300, 400, and 500°C are shown in Fig. 12. In these spectra, a broad sextet having a large magnetic hyperfine field was observed in the samples heat treated at 300°C and below, but only slightly in the samples heat treated at 400°C and above. This parallels what was observed visually when heat treated samples were exposed to air.

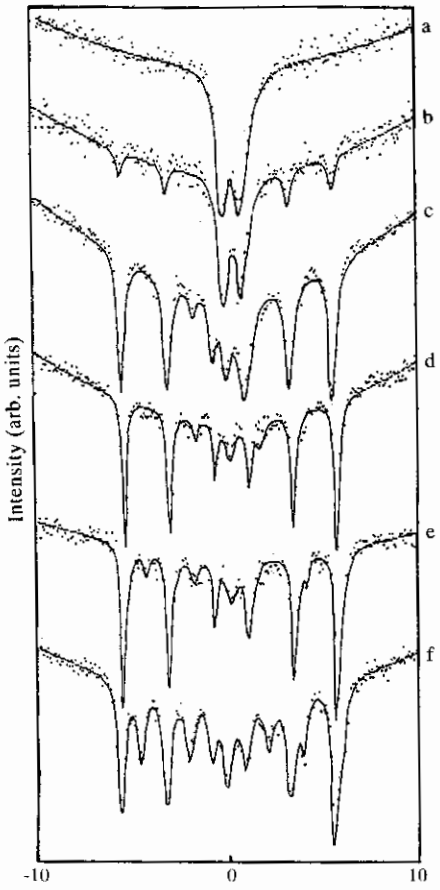

Fig. 11. Room temperature Mössbauer spectra for Fe/thiol samples (a) fresh and samples heat treated at (b) 200, (c) 300, (d) 400, (e) 500 and (f) 600°C.

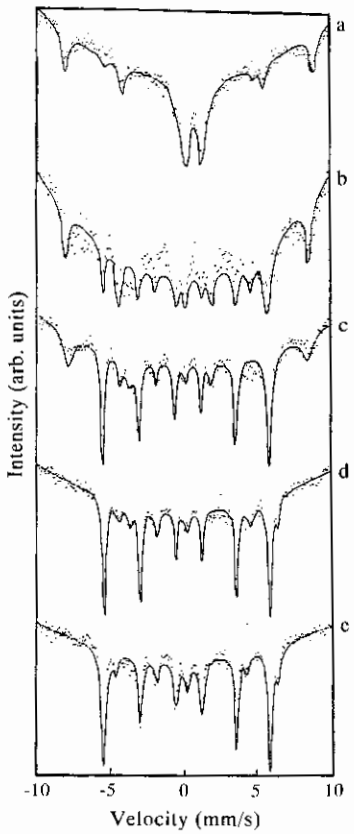

Fig. 12. Low temperature Mössbauer (77 K) spectra for Fe/thiol samples heat treated at (a) 100, (b) 200, (c) 300, (d) 400 and (e) 500°C.

Samples treated at temperatures of 100 to 300°C burned upon exposure to air. The samples heat treated at 400°C smoked slightly and samples treated at 500 and 600°C did not show any signs of oxidation when exposed directly to air.

From these data we believe that samples heat treated at 400°C and above are stable towards rapid oxidation. The major iron containing species present in these powders after heat treatment at these temperatures are α-Fe and FeS. As was noted earlier, a sample heat treated at 300°C did not show any indication of the formation of crystalline oxides after exposure to air for three months (Fig. 13).

Magnetic properties. SQUID magnetometry studies indicated that saturation magnetization M_s was 78 EMU g^{-1} at 10 K and decreased slightly to 75 EMU g^{-1} at 300 K for fresh Fe/thiol samples. This latter value is much lower than the bulk value of iron which is 220 EMU g^{-1} at room temperature. We were not surprised by this since the samples are made up of very small particles and iron does not account for the total mass of the sample.

Since the particles in the fresh samples were known to be less than 5 nm in diameter, we investigated the possibility of superparamagnetic behaviour. Plots of M vs H/T for data collected at 220 and 300 K did superimpose. However, hysteresis was observed. This indicates that the samples did not behave purely superparamagnetically even though the particle size was very small. As can be seen in the TEM photograph clustering of the small particles occurred in the fresh sample and this could be responsible for the deviations from superparamagnetic behaviour.

Because of the core/shell structure of the heat treated powders and the fact that FeS is an antiferromagnetic material, we believed that our powders might behave similarly to the Co/CoO system described in the background information. Therefore, we investigated the occurrence of shifted hysteresis loops for powders which had been heat treated at 300°C and above, that is, at temperatures at which FeS is known to be present in our samples. Samples were cooled to 10 K in an applied field of 10 kOe and the hysteresis loops measured. Only small shifts in the hysteresis loops of samples which had been heat treated at 300 to 600°C were observed. For example, a sample which had been heat treated at 300°C showed a 175 Oe shift while a sample treated at 600°C showed no shift at all. These shifts are an order of magnitude smaller than those observed in the Co/CoO system.[36] If the Neel temperature of FeS occurs above 300 K, then field cooling from room temperature to 10 K will not result in the alignment of the easy axis of magnetization of the antiferromagnetic surface layer with the ferromagnetic core and a shift in the loop will not be observed. FeS is reported to have a Neel temperature of 613 K,[8] however, this value is for pyrrhotite which actually has the formula $Fe_{1-x}S$ where $0 < x < 0.2$.[110,111] A search of the literature did not yield any information on the Neel temperature of troilite, FeS, which had been established by XRD and Mössbauer spectra as the phase which was present in our powders.

High temperature magnetic measurements using a VSM were carried out to investigate the magnetic behaviour of the samples above room temperature. Samples which were fresh or which had been heat treated up to 300°C showed a steady decrease in magnetization with temperature up to 800 K. However, samples which had been heat treated at 400–600°C had an inflection point in the plot of M vs T. This is illustrated in Fig. 14 for a sample heat treated

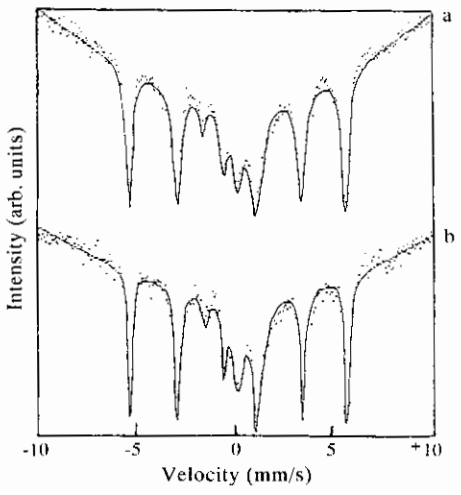

Fig. 13. Room temperature Mössbauer spectra of Fe/thiol sample heat treated at 300°C and exposed to air for (a) 1 day and (b) 3 months.

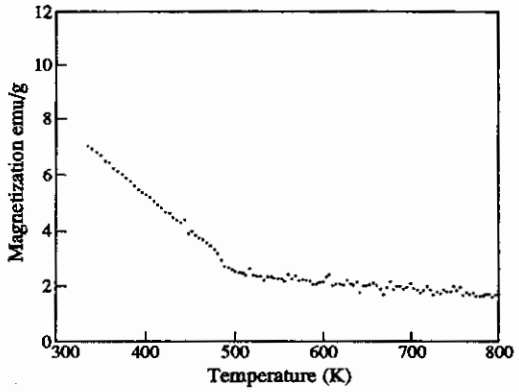

Fig. 14. M vs T for Fe/thiol samples prior heat treated to 600°C.

to 600°C. The temperature at which this abrupt change in magnetization occurred was at 490 K for the 400°C sample and 498 K for the samples heat treated at 500 and 600°C.

As the formation of FeS in our samples is believed to occur at treatment temperatures of 300°C and above, it is proposed that 400–499 K corresponds to the Neel temperature of the FeS in our powders. This also explains the fact that we did not see pronounced exchange interaction between the Fe and the FeS surface layer. Whether or not troilite actually has a lower Neel temperature than pyrrhotite or if this low value is a small particle effect, as was observed for FeF_2 discussed earlier, cannot be stated with certainty.

These fine powders did exhibit rather large coercivities which were observed to decrease with increasing particle size (determined from TEM photographic negatives). Figure 15 illustrates the change in H_c and M_s with particle size. There is a sharp change in the behaviour of these powders at a size of about 25 nm. The maximum in the coercivity appears at approximately the same size as that observed by Carmen and coworkers, who reported a maximum H_c of 1000 Oe for iron particles having a mean grain diameter of 25 nm.[112] At the same size at which H_c decreases M_s increases indicating a transition from single to multi-domain behaviour.[8]

We conclude that iron samples prepared in pentane and then trapped with 1-dodecanethiol are air sensitive as prepared but become stable towards oxidation after heat treatment to 400°C or above. The major products obtained after heat treating the powders are α-Fe and FeS according to Mössbauer and XRD spectra. TEM photographs suggest a core shell structure for particles after heat treatment to 300°C and above. It is proposed that these particles have an α-Fe core coated with a predominately FeS layer.

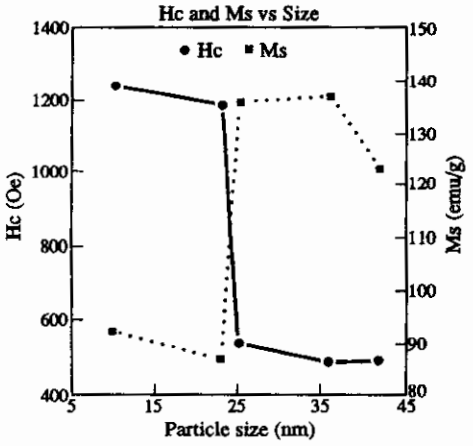

Fig. 15. Coercivity vs particle size for the Fe/thiol system.

According to differential scanning calorimetry (DSC), the iron/thiol powders begin to crystallize at 210–225°C. Since there is sulphur present in the sample, the formation of some Fe—S bonds must also occur and an additional exothermic peak at 300–325°C corresponds to the formation of FeS (this species was identified by XRD peaks in the spectrum of the sample heat treated at 400°C). The Mössbauer spectrum of the 400°C heat treated sample also shows the emergence of peaks due to FeS which are observed to become more intense after heat treatment at 500 and 600°C. Another broad exotherm observed at 400–450°C in the DSC may correspond to the decomposition of coordinated dodecanethiol fragments leading to the formation of the carbonaceous outer layer observed in the XPS spectra.

CONCLUSIONS

The clustering of metal atoms in cold matrices can be controlled somewhat by choice of matrix material ("solvent"), concentration and warm-up rate. During warm-up from 77 to 300 K particle growth is arrested because the larger the particle grows, the less mobile it becomes, and the more strongly solvated/ligated.

The solvents chosen always react with the growing clusters. The extent of reaction depends on the reactivity of the metal atom/cluster under study, and the solvent chosen. Alkanes are usually a good choice because even though reaction takes place, metal—hydride and metal—alkyl species can usually be eliminated by heat treatment since they are rather unstable. This approach can also be used to prepare bimetallic particles and core-shell structures.

In the current study it was found that: (1) Fe–hexane (or pentane) co-depositions led to extremely air-sensitve fine powders of iron of average crystallite sizes about 5 nm, and these particles exhibited superparamagnetic behaviour at room temperature. (2) A polar perfluorinated solvent, perfluorotri-n-butylamine (PFTA, "Fluoroinert"), reacted extensively with the growing Fe clusters, and the final product contained a small core of α-Fe surrounded by a thick layer of FeS, which in turn was coated with a C_xF_y layer. (3) Iron–silver co-depositions led to a mixture of morphologies, including Fe atoms isolated in silver, nanoscale Fe particles in silver, and separate Fe and Ag clusters. However, particles with core-shell morphology were unfortunately not the major product. (4) The most promising system was obtained by trapping iron clusters with a long

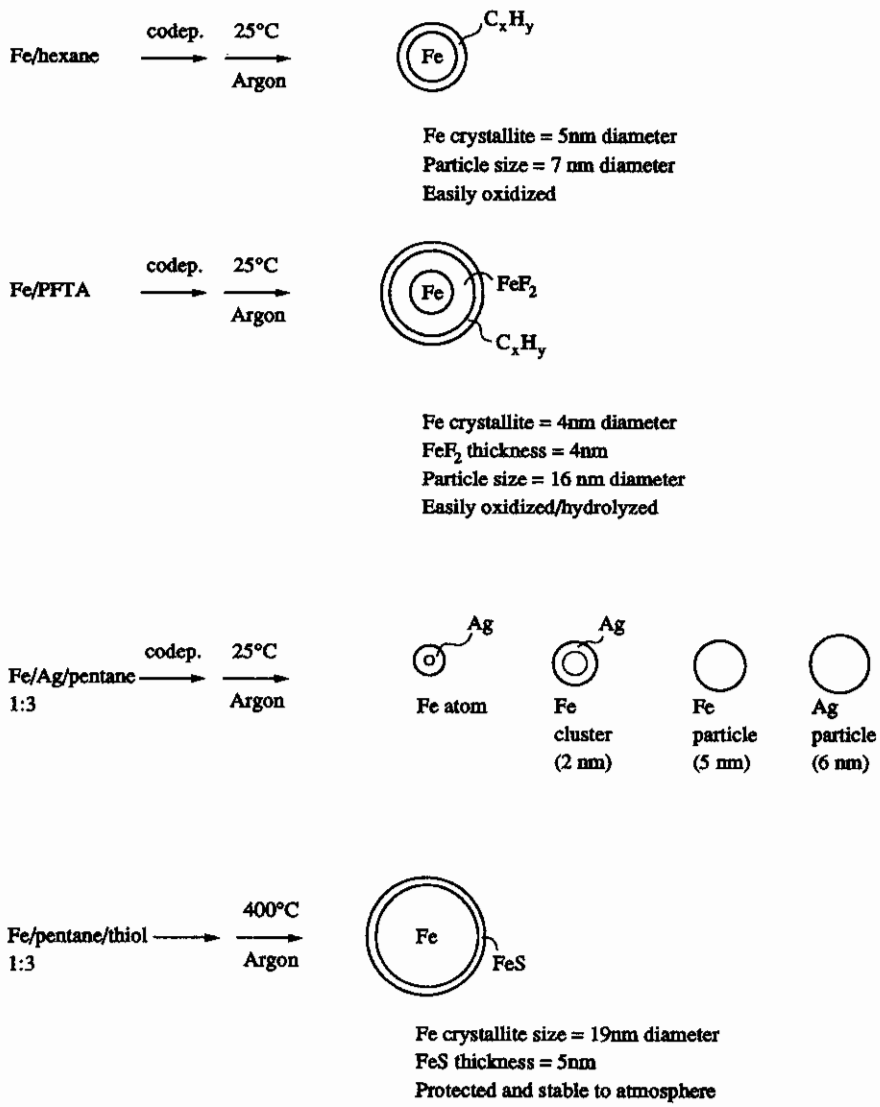

Fig. 16. A summary of morphologies for preparative procedures employed.

chain thiol. Upon heat treatment a Fe/FeS core-shell structure formed. In this way the Fe core was protected from environmental oxidation. Iron crystallite sizes could be controlled by heat treatment temperature and ranged from <5 to 40 nm. Magnetic properties were particularly interesting due to partial size variations, and exchange interaction between the ferromagnetic Fe core and antiferromagnetic FeS coating.

Figure 16 summarizes the transformations carried out and morphologies observed for selected conditions.

Acknowledgements—We thank Dr B.J. Tan and Professor S. Suib of the University of Connecticut for collecting XPS, SIMS, and Auger data and assisting with data interpretation. Also, we gratefully acknowledge the National Science Foundation (grants CHE-9106649 and CHE-9013930) for financial support.

REFERENCES

1. E. C. Theil, *ACS Symp. Ser.* 1988, **372**, 179.
2. J.A. Dumesic, H. Topsoe, S. Khanmouma and M. Boudart, *J. Catal.* 1975, **37**, 503.
3. A. Henglein, *Chem. Rev.* 1989, **89**, 1861.
4. M. Ozaki, *MRS Bulletin* December, 1989, pp. 35.
5. (a) Y.-X. Li and K. J. Klabunde, *J. Catal.* 1990, **126**, 173; (b) Y.-X. Li and K. J. Klabunde, *Hyperfine Inter.* 1988, **41**, 665.

6. (a) C. F. Kernizan, K. J. Klabunde, C. M. Sorensen and G. C. Hadjipanayis, *Chem. Mater.* 1990, **2**, 70; (b) S. C. Davis, S. J. Severson and K. J. Klabunde, *J. Amer. Chem. Soc.* 1981, **103**, 3024.
7. J. P. Jakubovics, in *Magnetism and Magnetic Materials, Institute of Metals*, Brookfield, VT (1987).
8. B. D. Cullity, in *Introduction to Magnetic Materials*, Addison-Wesley, Reading, MA (1972).
9. T. Ishikawa and E. Matijevic, *Langmuir* 1988, **4**, 26.
10. (a) R. Uyeda, *J. Cryst. Growth* 1974, **24**, 69; and (b) M. E. Tremblay, B. W. Smith, M. B. Long and J. D. Winefordner, *Spectroscopy Lett.* 1987, **20**, 311.
11. M. L. Mandich, V. E. Bondybey and W. D. Reents, *J. Chem. Phys.* 1987, **86**, 4245.
12. (a) W. R. Cannon, S. C. Danforth, J. H. Flint, J. S. Haggerty and R. A. Marra, *J. Amer. Ceramic Soc.* 1982, **65**, 324; (b) G. W. Rice and R. L. Woodin, *J. Am. Ceramic Soc.* 1988, **71**, C181.
13. (a) P. Fayet and L. Wöste, *Z. Phys.* 1986, **D3**, 177; (b) R. B. Wright, J. K. Bates and D. M. Gruen, *Inorg. Chem.* 1978, **17**, 2275.
14. Y. Liu, Q.-L. Zhang, F. K. Tittle, R. F. Curl and R. E. Smalley, *J. Chem. Phys.* 1986, **85**, 7434.
15. M.D. Morse, *Chem. Rev.* 1986, **86**, 1049.
16. K. LaiHing, R. G. Wheeler, W.L. Wilson and M.A. Duncan, *J. Chem. Phys.* 1987, **87**, 3401.
17. E. A. Rohlfing, D. M. Cox, R. Petkovic-Luton and A. Kaldor, *J. Phys. Chem.* 1984, **88**, 6227.
18. K. LaiHing, P. Y. Cheng and M. A. Duncan, *J. Phys. Chem.* 1987, **91**, 6521.
19. G. W. Rice and R. L. Woodin, *Proc. SPIE* 1984, 458.
20. (a) T. Miyahara and K. Kawakami, *IEEE Trans. Mag.* 1987, **MAG-23**, 2877; (b) E. Matijevic and P. Scheiner, *J. Colloid Interface Sci.* 1978, **63**, 509; (c) S. Hamada and S. Niizeki, Y. Kudo, *Bull. Chem. Soc. Jpn* 1986, **59**, 3443; (d) M. Ozaki, S. Krathovil and E. Matijevic, *J. Colloid Interface Sci.* 1984, **102**, 146.
21. (a) M. Boutonnet, C. Anderson and R. Carsson, *Acta Chem. Scand., Ser. A* 1980, **A34**, 639; (b) M. Boutonnet, J. Kizling and P. Stenius, *Colloid Surf.* 1982, **5**, 209; (c) N. Lufimpadio, J. B. Nagy and E. G. Derouane, in *Surfactants in Solution* (Edited by K. L. Mittal and B. Lindman), Vol. 3, pp. 1483–1497. Plenum Press, New York (1984).
22. (a) G. D. Stucky, *Navel Res. Rev.* 1991, **3**, 28; (b) R. D. Stramel, T. Nakamura and J. K. Thomas, *J. Chem. Soc. Faraday Trans.* 1, 1988, **84**, 1287.
23. (a) E. Z. Zuckerman, K. J. Klabunde, B. J. Olivier and C.M. Sorensen, *Chem. Mater.* 1989, **1**, 12; (b) G. Cardenas-Trivino, K. J. Klabunde and E. B. Dale, *Langmuir* 1987, **3**, 986; (c) K. J. Klabunde, H. F. Efner, L. Satek and W. Donley, *J. Organomet. Chem.* 1974, **71**, 309; (d) Y.-X. Li and K.J. Klabunde, *Hyperfine Int.* 1985, **41**, 665; (e) W. Yi, Y.-X, Li and K. J. Klabunde, in *ACS Symposium Series* 519, *Selectivity in Catalysis* (Edited by Steve Suib and M. Davis), Ch. 7, ACS Publication, Washington, D.C. (1993); (f) B. J. Tan, K. J. Klabunde and P. M. A. Sherwood, *Chem. Mater.* 1990, **2**, 186; (g) C. F. Kernizan, K. J. Klabunde, C. M. Sorensen and G. C. Hadjipanayis, *Chem. Mater.* 1990, **2**, 70.
24. C. P. Bean and I. S. Jacobs, *J. Appl. Phys.* 1956, **27**, 1448.
25. I. Nakatini, T. Furubayashi, T. Takahasi and H. Hanaoka, *J. Magn. Magn. Mater.* 1987, **65**, 261.
26. M. Hayashi, I. Tamura, Y. Fukano, S. Kanemaki and Y. Fujio, *J. Phys. C: Solid State Phys.* 1980, **13**, 681.
27. P. J. Picone, K. Haneda and A. H. Morrish, *J. Phys. C: Solid State Phys.* 1982, **15**, 317.
28. Z. O. Qui, Y. W. Du, H. Tang and J. C. Walker, *J. Appl. Phys.* 1988, **63**, 4100.
29. S. Gangopadhyay, G. C. Hadjipanayis, B. Dale, C. M. Sorensen, K. J. Klabunde, V. Papaefthymiou and A. Kostikas, *Phys. Rev. B* 1992, **45**, 9778.
30. J. Phillips, B. Clausen and J. A. Dumesic, *J. Phys. Chem.* 1980, **84**, 1814.
31. K. S. Suslick, S. B. Choe, A. Cichowlas and M. Grinstaff, *Nature* 1991, **353**, 414.
32. B. D. Cullity, in *Introduction to Magnetic Materials*, Addison-Wesley, Reading, MA (1972).
33. P. Weiss, *Compt. Rend.* 1906, **143**, 1136.
34. J. T. Michalak and R. C. Glenn, *J. Appl. Phys.* 1961, **32**, 1261.
35. K. Honda and K. Kaya, *Sci. Rep. Tohoku Imp. Univ.* (1), Dec. 1926, **15**, 721.
36. W. H. Meikeljohn and C. P. Bean, *Phys. Rev.* 1957, **105**, 904.
37. J. S. Kouvel, C. D. Graham Jr and I. S. Jacobs, *J. de Phys. et Radium* 1959, **20**, 198.
38. J. P. Jakubovics, in *Magnetism and Magnetic Materials, Institute of Metals*, Brookfield, VT (1987).
39. J. Frenkel and J. Dorfman, *Nature* 1930, **126**, 274.
40. E. C. Stoner and E. P. Wohlfarth, *Phil. Trans. R. Soc.* 1948, **A-240**, 599.
41. E. P. Wohlfarth, in *Magnetism III* (Edited by C. T. Rado and H. Suhl), Ch. 7, Academic Press, New York (1963).
42. E. E. Carmen, *Powder Met.* 1959, **4**, 1.
43. F. E. Luborsky and T. O. Paine, *J. Appl. Phys.* 1960, **31**, 685.
44. L. Neel, *C. R. Acad. Sci.* 1949, **228**, 664.
45. C. P. Bean and J. D. Livingston, *J. Appl. Phys.* 1959, **30**, 1205.
46. J. W. Niemantsverdriet, A. M. van der Kraan, W. V. Delgass and M. A. Vannice, *J. Phys. Chem.* 1985, **89**, 67.
47. R. L. Mössbauer, *Z. Phys.* 1958, **151**, 124.
48. R. L. Cohen, in *Applications of Mössbauer Spectroscopy*, (Edited by R. L. Cohen), Vol. I, Ch. 1, Academic Press, New York (1976).
49. (a) H. M. Gager and M. C. Hobson Jr, *Catal. Rev.* 1975, **11**, 117; (b) M. C. Hobson Jr, *J. Electrochem. Soc.* 1968, **115**, 175C.
50. R. W. Grant, in *The Mössbauer Effect and Its Application in Chemistry*, Ch. 3. ACS, Washington, D.C. (1967).

51. A. von Eynatten and H. E. Bömmel, *Appl. Phys.* 1977, **14**, 415.
52. R. C. Collins, *J. de Phys.* 1979, **40**, C2–36.
53. (a) K. Kimoto, Y. Kamiya, M. Nonoyama and R. Uyeda, *J. Appl. Phys.* 1963, **2**, 702; (b) A. Tasaki, S. Tomiyama, S. Iida, N. Wada and R. Uyeda, *J. Appl. Phys.* 1965, **4**, 707.
54. J. S. Van Wieringen, 1968, *Phys. Lett. A*, **26**, 370.
55. J. M. D. Coey and D. Khalafalla, *Phys. Status Solidi (a)*, 1972, **11**, 229.
56. S. Morup, H. Topsoe and J. Lipka, *J. de Phys.* 1976, **37**, C6–287.
57. I. Tamura and M. Hayashi, *J. Magn. Magn. Mater.* 1983, **31–34**, 945.
58. C. Wivel and S. Morup, *J. Phys. E* 1981, **14**, 605.
59. T. K. McNab, R. A. Fox and J. F. Boyle, *J. Appl. Phys.* 1968, **39**, 5703.
60. M. Eibschütz. and S. Shtrikman, *J. Appl. Phys.* 1968, **39**, 997.
61. W. Schuele, S. Shtrikman and D. Treves, *J. Appl. Phys.* 1965, **36**, 1010.
62. (a) G. K. Wertheim and J. P. Remeika, *Phys. Lett.* 1964, **10**, 14; (b) S. Ofer, B. Khergen, M. Kakavy and I. Nowik, *Phys. Lett.* 1964, **11**, 205.
63. D. W. Collins, J. T. Dehn, L. N. Mulay, in *Mössbauer Effect Methodology: Proceedings at the Symposium on Mössbauer Effect Methodology*, pp. 103–122. Plenum Press, New York (1967).
64. K. J. Klabunde, P. L. Timms, P. S. Skell and S. D. Ittel, *Inorg. Syn.* 1979, **19**, 59.
65. (a) K. J. Klabunde, Y.-X. Li and B. J. Tan, *Chem. Mater.* 1991, **3**, 30; (b) K. J. Klabunde and Y. Tanaka, *J. Molec. Catal.* 1983, **21**, 57; (c) Y.-X. Li, Y.-F. Zhang and K. J. Klabunde, *Langmuir* 1988, **4**, 385; (d) S. C. Davis and K. J. Klabunde, *Chem. Rev.* 1982, **82**, 153.
66. P. C. Hiemenz, *Principles of Colloid and Surface Chemistry*, Marcel Dekker, New York (1986).
67. K. A. Easom, Ph.D. Thesis, Kansas State University (1992).
68. S. Nafis, Z. X. Tang, B. Dale, C. M. Sorensen, G. C. Hadjipanayis and K. J. Klabunde, *J. Appl. Phys.* 1988, **64**, 5835.
69. N. N. Greenwood and T. C. Gibb, in *Mössbauer Spectroscopy*, Chapman Hall, London (1971).
70. H. M. Gager and M. C. Hobson Jr, *Catal. Rev.* 1975, **11**, 117.
71. (a) G. Constabaris, R. H. Lindquist and T. Takada, *J. de Phys.* 1979, **40**, C2–153; (b) Connell, G. and J. A. Dumesic, *J. Catal.* 1986, **102**, 216.
72. J. W. Niemantsverdriet, A. M. van der Kraan, W. V. Delgass and M. A. Vannice, *J. Phys. Chem.* 1985, **89**, 67.
73. T. Shigematsu, Y. Bando and T. Takuda, *J. de Phys.* 1979, **40**, C2–453.
74. J.-S. Jiang, X.-L. Yang, L.-W. Chen and N.-F. Zhou, *Appl. Phys. A*, 1988, **45**, 245.
75. (a) L. B. Twu, S. Borcar, D. Bianchi and C. O. Bennett, *J. Catal.* 1984, **87**, 36; (b) J. A. Amelse, J. B. Butt and L. H. Schwartz, *J. Phys. Chem.* 1978, **82**, 558.
76. S. C. Davis, S. J. Severson and K. J. Klabunde, *J. Amer. Chem. Soc.* 1981, **103**, 3024.
77. C. Heck, *Magnetic Materials and their Applications*, pp. 172–175. Crane, Russak and Co., New York (1974).
78. Z. O. Qui, Y. W. Du, H. Tang and J. C. Walker, *J. Appl. Phys.* **63**, 4100, (1988).
79. Fluoroinert, perfluor(n-tributyl)amine, supplied by 3M.
80. M. D. Veremeyenko, I. F. Alenchikova and V. I. Nejedov, *Poverkhnost* 1985, **5**, 123.
81. *Handbook of X-ray Photoelectron Spectroscopy*, (Edited by G. E. Mullerberg), Perkin-Elmer, Eden Prairie, MN, (1970). fluorine: pp. 44–45. iron: pp. 76–77. carbon: pp. 38–39.
82. S. Ramasamy, J. Jiang, H. Gleiter, R. Birringer and U. Gonser, *Solid State Commun.* 1990, **74**, 851.
83. G. Ferey, A. M. Leclerc, R. de Pape, J. P. Mariot and F. Varret, *Solid State Commun.* 1979, **29**, 477.
84. S. Swanepoel and C. M. Stander, *J. Phys. Chem. Solids* 1987, **48**, 275.
85. T. Shigematsu, Y. Bando and T. Takada, *J. Physique* 1979, **40**, C2–153.
86. M. E. Lopez-Herrera, F. Varret, Y. Calage and G. Ferey, *J. Mag. Mag. Mater.* 1984, **44**, 304.
87. P. L. Crouse and C. M. Stander, *J. Phys. Chem. Solids* 1988, **49**, 1145.
88. Y. Macheteau, J. Gillardeau, P. Plurien and J. Ouder, *Oxid. Metals* 1972, **4**, 141.
89. (a) Y.-X. Li, Y.-F. Zhang and K. J. Klabunde, *Langmuir*, 1988, **4**, 385; (b) Y.-X. Li and K. J. Klabunde, *J. Catal.* 1990, **126**, 173
90. G. N. Glavee, C. F. Kernizan, K. J. Klabunde, C. M. Sorensen and G. Hadjipanayis, *Chem. Mater.* 1991, **3**, 967.
91. M. Hansen, K. Aderko, K., in *Constitution of Binary Alloys*, pp. 20. McGraw-Hill, New York, (1958).
92. G. I. Petreko, *Z. anorg. Chem.* 1907, **53**, 215.
93. G. Tammau and W. Oelsen, *Z. anorg. Chem.* 1939, **186**, 277.
94. G. Longworth and R. Jain, *J. Phys. F*, 1978, **8**, 993.
95. (a) K. Sumiyama, N. Kataoka and Y. Nakamura, *Jpn J. Appl. Phys.* 1988, **27**, 1693; (b) C. L. Chien and K. M. Unruh, *Phys. Rev. B* 1983, **28**, 1214.
96. M. Tako and H. Senno, *J. Magn. Magn. Mater.* 1983, **31–34**, 949.
97. N. Kataoka, K. Sumiyama and Y. Nakamura, *J. Phys. F*, 1985, **15**, 1405.
98. N. Kataoka, K. Sumiyama and Y. Nakamura, *Trans. Jpn Inst. Metals*, 1985, **26**, 703.
99. K. L. Chopra, in *Thin Film Phenomena*, pp. 17. McGraw-Hill, New York, (1969).
100. V. Nakamura, K. Sumiyama and N. Kataoka, *Hyperfine Int.* 1988, **41**, 599.
101. C. Kittel, In *Introduction to Solid State Physics*, 6th ed., p. 588. John Wiley, New York, (1986).
102. F. Schmidt, A. Quazi, A. X. Trautwein, G. Doppler and H. M. Ziethen, *Z. Phys. D* 1986, **3**, 303.
103. C. Wivel and S. Morup, *J. Phys. E* 1981, **14**, 605.
104. (a) J. S. Van Wieringen, *Phys. Lett.* 1968, **26**, 370:

(b) I. Tamura and M. Hayashi, *J. Magn. Magn. Mater.* 1983, **31–34**, 945.
105. H. Topsoe and M. Boudart, *J. Catal.* 1973, **31**, 346.
106. C. D. Bain and G. M. Whitesides, *J. Phys. Chem.* 1989, **93**, 1670.
107. J. J. Hickman, D. Ofer, Z. Chaufeng, M. S. Wrighton, P. E. Laninis and G. M. Whitesides, *J. Am. Chem. Soc.* 1991, **113**, 1128.
108. N. E. Erickson, *ACS Advances in Chem. Ser.* 1967, **68**, Ch. 6.
109. N. N. Greenwood and T. C. Gibb, in *Mössbauer Spectroscopy*, Chapman Hall, London (1971).
110. E. C. Sprenkel-Segel and S. S. Hanna, *Geochim. Cosmochim. Acta* 1964, **28**, 1913.
111. S. Yokoyama, R. Yoshida, H. Narita, K. Kodaira and Y. Mackawa, *Fuel* 1986, **65**, 164.
112. E. H. Carmen, *Powder Met.* 1959, **4**, 1.